Holocene East African monsoonal variations recorded in wave-dominated clastic paleo-shorelines of Lake Abhe, Central Afar region (Ethiopia & Djibouti)

Carlo Mologni, Laurent Bruxelles, Mathieu Schuster, Gourguen Davtian, Clément Ménard, François Orange, Cécile Doubre, Jessie Cauliez, Haftom Berhane Taezaz, Marie Revel, et al.

To cite this version:

Carlo Mologni, Laurent Bruxelles, Mathieu Schuster, Gourguen Davtian, Clément Ménard, et al.. Holocene East African monsoonal variations recorded in wave-dominated clastic paleo-shorelines of Lake Abhe, Central Afar region (Ethiopia & Djibouti). Geomorphology, 2021, 391, pp.107896. 10.1016/j.geomorph.2021.107896 . hal-03386578

HAL Id: hal-03386578
https://hal.science/hal-03386578

Submitted on 22 Aug 2023

Holocene East African monsoonal variations recorded in wave-dominated clastic paleo-shorelines of Lake Abhe, Central Afar region (Ethiopia & Djibouti)

Carlo Mologni[1, 4]*, Laurent Bruxelles[2], Mathieu Schuster[3], Gourguen Davtian[4], Clément Ménard[5], François Orange[6], Cécile Doubre[3], Jessie Cauliez[7], Haftom Berhane Taezaz[8], Marie Revel[1], Lamya Khalidi[4]

[1] Université Côte d'Azur, CNRS, Observatoire de la Côte d'Azur, IRD, Géoazur, 06905 Sophia Antipolis, France

[2] Université Toulouse Jean Jaurès, CNRS, TRACES - UMR5608, 31058 Toulouse, France - GAES, University of the Witwatersrand, Johannesburg, South Africa

[3] Université de Strasbourg, CNRS, Institut Terre et Environnement de Strasbourg, UMR 7063, 5 rue Descartes, Strasbourg F-67084, France

[4] Université Côte d'Azur, CNRS, CEPAM – UMR 7264, 06300 Nice, France

[5] Centre Français des Etudes Ethiopiennes (CFEE), P.O. Box 5554, Addis-Ababa, Ethiopia

[6] Université Côte d'Azur, CCMA, 06100, Nice, France

[7] Université Toulouse Jean Jaurès, TRACES - UMR5608, CNRS, 31058 Toulouse, France

[8] Authority for Research and Conservation of Cultural Heritages of Ethiopia, Addis-Ababa, Ethiopia

*Corresponding Author: mologni@geozur.unice.fr

Abstract

In tropical Africa, Late Pleistocene -Holocene climatic fluctuations heavily impacted the continental hydro-systems. The timing and magnitude of 'African Humid Period' hydrological dynamics (AHP; ~14.8 – ~5.5 ka BP) are not yet fully understood due to the extreme variability in African geomorphic patterns and the complex network of past air convergence boundary shifts. The investigation of the functioning of specific hydro-sedimentary basins is needed to improve our knowledge on the AHP spatial and chronological patterns over the continent. In this paper we present a revised Holocene lake level curve of Lake Abhe: an endorheic basin situated in the Afar Depression at the northern extremity of the East African Rift System (EARS). Located at the boundary of the Red Sea and the Indian and Atlantic Oceans' air moisture mass fluxes, the Lake Abhe watershed represents a system sensitive to changes in Northeast African hydro-climate. Based on numerous littoral lacustrine geomorphic features and 53 related radiocarbon ages on stromatolites and nearshore deposits, we have defined the main Holocene lake highstands proposing a detailed paleo-shoreline record. The first rise in water level is dated to ~11.1 ka cal. BP, while the Maximal Holocene Highstand Shoreline (~420 m a.s.l.) was rapidly reached around ~10 ka cal. BP. Evidence of the impact of the 8.2 ka North Atlantic cooling event is recognised with slow lake level regression until ~8.3 ka cal. BP and with an abrupt drop at ~8 ka cal. BP. The resurgence of humid conditions was recorded from ~7.7 ka cal. BP to ~4.6 ka cal. BP. Radiocarbon ages on littoral materials allow us to propose a Holocene subsidence rate of the Abhe basin axial valley. Furthermore, multiphase sill overflow incisions towards the downstream Hanle basin and transient fluvial connectivity with the upstream Ziway-Shala basin, indicate strong geomorphic controls on lake highstand elevations. In summary, Lake Abhe Holocene fluctuations are the result of combined hydro-climatic, tectonic and local geomorphic controls. However, the confrontation with others East African basins allows us to discuss the transport of moisture masses dynamics into the northern EARS during the Holocene.

Keywords: East African Rift System, Central Afar Region, Lake Abhe, Paleo-shorelines, African Humid Period, Holocene, 8.2 ka event, Tectonic deformation

1 – Introduction

Today, the tropics concentrate the maximum amount of solar energy and redistribute it in the form of air and moisture masses to latitudes between 30° N and 30° S by atmospheric and oceanic circulation (https://earthobservatory.nasa.gov/features/EnergyBalance/page3.php). The intertropical solar-irradiation-induced precipitation/evaporation balance is at the base of Earth's atmospheric convection, and is thus considered one of the main driving processes of global climate evolution (Mohtadi et al., 2016).

From the Late Pleistocene to the Mid-Holocene periods, Africa was the theatre of significant changes in hydro-climatic conditions, which mainly followed precessional pacing (i.e., every 21,000 years; (Rossignol-Strick et al., 1982; Mohtadi et al., 2016; Skonieczny et al., 2019). From ca. 14.8 to 5.5 ka, the precession-driven increase of the northern hemisphere insolation magnitude seems to have been at the origin of the northward migration of the rainfall belt associated with the Intertropical Convergence Zone (ITCZ; deMenocal et al., 2000; Haug, 2001; Viste and Sorteberg, 2013). This period, referred to as the African Humid Period (AHP; deMenocal et al., 2000; Tierney et al., 2011), is characterized by enhanced precipitation in the tropics, the northward spread of vegetation cover (Hopcroft et al., 2017) and the massive reactivation of fluvial systems (Revel et al., 2015; Schefuß et al., 2016; Mologni et al., 2020) leading to the development of numerous lakes (Kutzbach and Street-Perrott, 1985; Gasse, 2000; Holmes and Hoelzmann, 2017). However, the general timing (onset and termination) and timing offsets of the AHP between Western and Eastern Africa, as well as between the Sahelian and Equatorial latitudes, need to be fully understood (deMenocal et al., 2000; Shanahan et al., 2015; Collins et al., 2017). The establishment of short-term (200-400 yr) African arid episodes, likely synchronous with the North Atlantic cooling events (HE1, YD, 8.2, 4.2 ka events; Rohling and Pälike, 2005; Collins et al., 2013, 2013; Rasmussen et al., 2014), bring to question the causal link between high and low latitudes, the role of the tropics in these cooling episodes (Clement et al., 2001; Davies et al., 2014), the mechanisms of the AHP (Shanahan et al., 2015), and the local non-linear response of African sedimentary basins to global climatic trends.

The numerous lakes of the 3000 km-long and N-S-tending East African Rift System (EARS) have proven to be excellent recorders of past climate evolution, providing both long and high-resolution archives (Gasse, 2000). However, the extensional tectonics (Déprez et al., 2013; Stamps et al., 2014, 2020) coupled with the extreme contrast between high precipitation rates in the highland catchment zones and high evaporation in the lowlands (‘amplifier lake’ patterns; Trauth et al., 2010) may induce a modulated response of lacustrine hydro-sedimentary systems to atmospheric inputs from continental climatic change. During the AHP, the enhanced atmospheric pressure gradient between the East African Monsoon and the Indian Summer Monsoon (ISM) would have led to an eastward migration of the Congo Air Boundary (CAB; Camberlin, 1997; Braconnot et al., 2008). These patterns induced an incursion of the West African Summer Monsoon (WAM) air masses along the EARS, causing a non-linear response of hydro-sedimentary systems to ITCZ north-south oscillations (Fig. 1a; Hailemichael et al., 2002; Tierney et al., 2011; Costa et al., 2014; Junginger et al., 2014). The acquisition of paleo-hydrological data from southern to northern EARS ranges adds relevant information to our understanding of moisture mass convergence zone dynamics during the AHP, which would have impacted, sometimes over the course of a few hundred years, the equilibrium and paleoenvironmental stability of ancient ecosystems.

The Abhe Lake basin, located at the northern extremity of the EARS (~12° N), is the widest and longest rift-controlled sedimentary basin of the Afar Depression. It derives its source in the Ethiopian Highlands (Fig. 1b, 1c). Currently reduced to a small (~350 km^2) and shallow (max. depth <30 m) waterbody (Wood and Telling, 1988), Lake Abhe experienced a highstand resulting in a large freshwater lake during the Early Holocene (~7000 km^2 and ~230 m max. depth; Gasse, 1975; Khalidi et al., 2020). The fluctuations of Lake Abhe's water level seem to follow the main AHP dry-wet oscillations (Gasse, 2000), producing some very marked littoral geomorphic features. Although they represent a reliable indicator of the paleo-hydrological evolution history of the basin, these littoral geomorphic features have never been documented or investigated in the Abhe region prior to this study. Deciphering the precise control of geomorphic systems over both hydro-climatic and geodynamic forcing is essential for a more robust interpretation of past climate-change data.

In the 1970s, Gasse and colleagues documented the paleoecological and lake level history of Lake Abhe based on lacustrine nearshore and offshore deposits (Rognon and Gasse, 1973; Gasse, 1975, 1977; Gasse and Street, 1978; Gasse et al., 1980). In this study we update and improve knowledge of Lake Abhe's paleo-hydrological fluctuations with better chronological and spatial control, and through a consideration of the effects of tectonic and geomorphic processes on past hydrological variations. We present a hydro-climatic record established using multiple paleo-shoreline geomorphic features spanning the last ~11 ka of Holocene Lake Abhe. Our record is age-controlled by 53 new and existing dates on foreshore/nearshore carbonate deposits such as stromatolites and *Melanoides tuberculata* shells. With the aim of determining the precise paleo-hydrological history of Holocene Lake Abhe, our results are combined with tectonic deformation kinematics data in order to take neo-tectonic control and deformation of the investigated geomorphic markers into account. New archaeological and perilacustrine sedimentary sequence chronologies provided in Khalidi et al. (2020) are cross-referenced with our data to better constrain lake-level reconstruction. Furthermore, earth surface processes which may have affected lake hydrological fluctuation dynamics (e.g. overflow sill incision, temporary fluvial interconnection with adjacent basins) are documented and discussed in the text.

Finally, our study is compared with other regional lacustrine paleo-hydrological records with the aim of estimating the influence of monsoonal variations on a N-S transect of the EARS during the Holocene period.

2- Regional settings

2.1 – Volcano-Tectonic control of the Abhe basin formation

Lake Abhe is located in the southeastern part of the Tendaho-Gobaad graben, which is the widest and longest basin within the Afar Depression. The extensional tectonics occurring in the Afar are associated with the triple junction of the divergent Somalian, Arabian and Nubian plate boundaries (Fig 1b). Over its 1.8 Myr-long development, the Tendaho-Gobaad graben has been the locus of interactions between three extensional systems related to the EARS, the Red Sea and the Aden ridges (Manighetti et al., 2001; Audin et al., 2004). It is considered the southwestern tip of the Red Sea propagating on land (Nubia-Arabian boundary), overlapping with the Aden Ridge (Somalia-Arabian boundary), while the extensional structures related to the northern tip of the EARS are observed in its southern margin along the Main Ethiopian Rift (MER; Fig 1c; Acton et al., 1991).

East African continental rifting began between ~31 and ~28 Ma following the emplacement of the flood basalts traps forming the Ethiopian and Yemeni high plateaus (current highlands, Hofmann et al., 1997; Tiercelin and Lezzar, 2002; Macgregor, 2015). Soon after, starting around ~25 to ~20 Ma, continental extension formed the large escarpments bounding the Afar Depression and developed the filling of large Miocene basins. The Stratoid series, a 1.5-km-thick basaltic sequence which covers most of the Afar region, was dated between 4.4 Ma and 0.4 Ma (Kidane et al., 2003; Varet, 2018). From 1.8 Ma, continental extension in the Central Afar was focused across several NNW to NW-trending active rift segments, concentrating tectonic deformation and, in most cases, magmatic activity. They formed a complex network of normal faults and several sub-rifts, horsts and grabens, to which the Tendaho-Gobaad graben belongs (Abbate et al., 1995). Many fissural volcanic flows related to the emplacement of the Stratoid series occurred between ~2 and ~0.5 Ma across the Tendaho-Gobaad graben, evidencing the link between the outflows of Stratoid magma and the collapse of the Tendaho-Gobaad graben (Acocella, 2010). Holocene rifting activity is evidenced by some volcanic cones and domes associated with NNW-trending sub-rifts in its northern part (Fig 1c; Barberi and Varet, 1977; Manighetti et al., 1998), and by the probable NE tilting of the basin plain proposed by Gasse (1975). This recent surface subsidence would have induced the capture of the Awash River (Gasse, 1975; Fig 1) leading to the current hydrological basin patterns. From recent geodetic studies (Doubre et al., 2017), the current NE-trending extension across the Tendaho-Gobaad graben does not exceed 7 mm/yr. The subsidence velocity of the inner floor cannot be easily estimated and no clear current slip on the bounding normal faults of the graben is detected from long InSAR time series (Pagli et al., 2014; Doubre et al., 2017). Temtime et al. (2018) identified an elongated NE-trending zone of present day subsidence reaching ~4 cm/yr over the 2004-2010 period from InSAR data, which they attributed to magmatic and hydrothermal activity below the basin.

These data indicate how tectonic control represents the primary driver of large-scale landform-formation-processes of the Abhe Lake basin. The strong extensional deformation of the crustal layer would have affected the sedimentogenetic processes and the organization of the lacustrine-induced morphological elements investigated in this study. However, the strong impact of past hydrological dynamics on sedimentary East African systems produced a considerable imprint on landscape morphologies (Nilsson, 1940; Garcin et al., 2012; Melnick et al., 2012).

2.2 – Hydro-climatic control of the Abhe basin and previous paleo-lacustrine studies

The Abhe basin sedimentary system receives its water catchment from the Awash River which derives its source in the region of highland Ethiopia southwest of Addis Ababa. Freshwater supplies are mainly generated by African monsoon precipitation on the Ethiopian Highlands during the rainy season from June to September (200 to 300 mm/month). Air moisture flows moving into northern Ethiopia originate from the Gulf of Guinea, the Indian Ocean, the Red/Mediterranean Seas and the Arabian Peninsula (Viste and Sorteberg, 2013).

Descending the highlands, the Awash River is joined by many affluent rivers until it meets the Lower Awash Plain (4000 km^2), which coincides with the northwestern part of the Tendaho-Gobaad graben. Here, the river course continues, without any perennial freshwater supply, to Gamari and Afambo Lakes (339 m a.s.l.) and to its final destination, endorheic Lake Abhe (Fig 1c; 240 m a.s.l.). Over the course of one year, the Abhe basin is seasonally supplied by smaller local catchments at the extremities of the graben, namely the Gobaad (South-East) and the Logiya (North-West) Rivers. Presently, the Central Afar region is characterized by a hyper-arid climate with 200 mm/yr precipitation and with an evaporation rate of 3500 mm/yr (Rognon and Gasse, 1973; Gasse, 1990; Varet, 2018).

At the tropics, monsoonal rainfall magnitude variations over the last 1 Ma have been attributed to the northward migration of the rainfall belt associated with the ITCZ together with precession-driven insolation changes (deMenocal et al., 2000; Gasse, 2000; Tuenter et al., 2003; Mohtadi et al., 2016; Lamb et al., 2018; Skonieczny et al., 2019). The large offset between the local precipitation and evaporation rates indicates that the orbital-induced monsoon activity in the Ethiopian highlands was primarily responsible for the hydro-sedimentary balance which generated the Late Pleistocene-Holocene synthems of the Abhe basin.

Except for a few Mio-Pliocene sequences located along the margins of the Afar Depression (Tiercelin, 1981; Gasse, 1990), the lacustrine sedimentary accumulation in the Central Afar region began during the Early Pleistocene (Gasse et al., 1980; Boucaurt et al., 1985), which seems synchronous with the Tendaho-Gobaad graben formation. However, sedimentary deposits developed within a topography similar to the current one started around 130 ka BP (Fontes and Pouchan, 1975; Gasse, 1975).

The first research conducted on Abhe basin sedimentary formations occurred in the 1970s and was focused on paleoecological reconstruction from deep (offshore) lacustrine deposits (Faure et al., 1971; Rognon and Gasse, 1973; Gasse, 1975, 1977). Three main lacustrine sedimentary sequences spanning 100 to 3 ka BP, were identified by Gasse (1977) based on study of exposed sections and offshore sediment cores: ~100-70 ka BP (Abhe I), 60-18 ka BP (Abhe II - Abhe III), and 10-4 ka BP (Abhe IV - Abhe V; Fig. 1c) corresponding to the AHP (~14.8 and ~5.5 ka; Shanahan et al., 2015).

Gasse (1975, 1977)reconstructed past Lake Abhe highstands on the basis of conventional radiocarbon ages and elevations from nearshore to offshore carbonate deposits, with little link to paleo-shoreline morpho-sedimentary structures and dynamics. A recent revision of these previous data with the integration of new calibrated ages performed on littoral carbonates and archaeological assemblages has led to the definition of a new water-level variation curve for Holocene Lake Abhe (Khalidi et al. 2020). In this study, we have further developed this approach with the aim of reconstructing Holocene monsoon-induced paleo-hydrological variations in the Lake Abhe basin with higher precision. During three survey campaigns (2018-2020), we documented different littoral morpho-sedimentary features with specific regard for a wide range of littoral-related geomorphic and depositional environments such as wave abrasion platforms/notches, overflow sill incisions, beach ridges, Gilbert-deltas, pedological horizons, gravity-induced deposits and fluvial or fluvio-lacustrine deposits. This approach, combined with a chronology assured by more than fifty radiocarbon ages on littoral carbonates, allows us to indicate the precise paleolake outlines and elevations and their relation to volcano-tectonic rifting-related deformation.

3 – Methodology

3.1 – Differential GPS (DGPS) survey and Digital Elevation Model (DEM) calibration

3.1 – DGPS survey and DEM calibration

During the 2018-2020 field campaigns, a large survey over the entire Abhe basin focused on the identification and GPS measurement of its littoral morpho-sedimentary and geomorphic elements. The detailed description and definition of the precise geomorphic elements considered as paleo-shoreline markers are provided in the results section 4.1 and in Sup. Mat. A. Additionally, in order to provide more accurate elevations from new GPS plots, and with the aim of testing and validating our previous measurements and calibrating the elevation data from Gasse (1975), a systematic DGPS survey was performed using the Trimble Geo 7X differential GPS, with a double frequency receptor (L1 = 1575.46 MHz, L1 = 1227.60 MHz). The vertical standard deviation of our measurements range between 1 and 2 cm. This analytical value error is similar to the Trimble error value. Due to the quasi-absence of geodetic reference points in the investigated region and with the aim to validate our elevation measurements, we compared our DGPS measurements with elevations from 2 DEMs: a total of 54 DGPS measurements were compared with SRTM® (www2.jpl.nasa.gov/srtm) and TanDEM-X (https://tandemx-science.dlr.de; Rizzoli et al., 2017) DEMs (Fig 2). Results show generally accurate elevations from the SRTM® (30 m resolution), however, they do not follow the homogeneity of DGPS measurements (Fig 2). In contrast, elevations extracted from the TanDEM-X data (12m resolution; Rizzoli et al., 2017) are more coherent with the DGPS data but with a systematic offset of -10 m (Fig 2). The elevation differences between our DGPS and the TanDEM-X data (with a +10 m offset applied) never exceed ~5 m (1.7 m average), while the differences with the STRM data sometimes reach ~10 m (2.3 m average). Taking into account the precision required for the elevation measurements, as well as the coarse sampling resolution of the SRTM DEM, the TanDEMx (+10 m offset) was preferred for the calibration of the GPS measurements obtained from three years of field campaigns and from previous location data provided in Gasse (1975). For each surveyed site (see 4.2.1), a topographic profile was generated with the location of geomorphic features (Supp. Mat. A), providing support for each paleo-shoreline level definition (see 4.2.2).

3.2. - Age control

With the aim of proposing a robust age model of the main paleo-shorelines recorded across the Lake Abhe basin, a calibration was performed on 18 AMS ^{14}C conventional ages on stromatolites, 9 on nearshore deposits and 26 on selected ages published in Gasse (1975).

The revision of previous Holocene Abhe paleolake water level data is based on the calibration and the re-calculated DEM elevations of ^{14}C ages on nearshore carbonate deposits published by Gasse (1975). The 26 published ages were selected according to the following criteria: a) only ages from littoral lacustrine (nearshore) material from the Abhe basin were considered; b) using stratigraphic information provided by Gasse (1975), inversed ages or ages from reworked sediments were not considered for the age model building; c) ages from paleo-shores of residual lakes were not considered (e.g., Gamari or Gargori residual lakes, Fig 4a); d) ages with incomplete geographic location (incomplete coordinates) do not allow a proper correlation with the DEM processing data and were not used for the model building; e) ages on archaeological material were not considered. The selected results are presented in Tab 1.

The age calibration (Tab 1) was performed using the OxCal 4.3 program (Bronk Ramsey, 2001). For conventional ages on littoral lacustrine carbonates, the calibration parameters were selected from the IntCal13 atmospheric calibration curve (Reimer et al., 2013). Considering that the estimated reservoir age effect for Early Holocene biogenic lacustrine carbonates is <100 yrs (Khalidi et al., 2020), which remains lower than the majority of the age standard deviations, no reservoir correction was applied.

We are aware that a reservoir age definition based on a single parallel dating is insufficient. However, comparison and cross-reference with archaeological data from littoral sequences presented in Khalidi et al. (2020) helped us to constrain possible reservoir age effect anomalies (see Section 5.2). The ages considered here used 95.4% ranges and are reported in median ka cal. BP (calibrated kilo annum before 1950).

4 – Results

4.1 - Paleo-shoreline geomorphic features of the Lake Abhe basin

Over the ~200-km-wide Abhe basin, more than one hundred littoral lacustrine geomorphic features were identified and mapped during the survey campaigns (2018-2020; Sup. Mat. A). The detection of more or less pronounced wave-cut abrasion features, typical beach pebble band concentrations, and continuous paleo-beach ridges, combined with other shore-related morpho-sedimentary facies (Gilbert-type deltas), ascribes the Abhe paleolake to the wave-dominated clastic shoreline lake-type as defined by Schuster and Nutz (2018).

In this section, we first describe and define the geomorphic marker types observed in the field. We then present each surveyed site together with the list of shorelines. Finally, we summarize the dataset of paleo-shorelines recognized across the Abhe basin.

4.1.1 – Wave-cut and overflow abrasion platforms

Wave energy enhanced by wind direction and magnitude can produce more or less developed shore platforms, abrasion ramps or cliff notches (Schuster et al., 2003; Trenhaile, 2015). The maximal estimated extension of the Holocene Lake Abhe waterbody (7000 km^2; Gasse 1975) presents the conditions to produce well-defined littoral abrasion features on clastic supports.

Throughout the Abhe basin, abrasion platforms and notches vary in relation to lateral changes in rock resistance. Wave-cut abrasion platforms that developed in acidic volcanic contexts such as rhyolitic domes and associated eruptive material (ignimbrite and pyroclastic rocks) are more pronounced, horizontally shaped, and frequently associated with well-developed cliff notches (Fig 3.a). Most wave-cut abrasion platforms that developed on basaltic stratoid series outcrops present a sub-horizontal or seaward-sloping shore morphology (gently sloping abrasion platforms as defined by Sunamura (1992) without any cliff notch features; Fig 3.b). The width of sub-horizontal abrasion platforms on rock outcrops can vary between ~10 and ~200 m, while when wave-cut incision occurs on pre-existing sedimentary deposits, the platform can achieve up to 1 km in width (Fig 3.c). Abrasion platform shape and dimension are even determined by long-term exposure to wave erosion, lake waterbody amplitude, which coupled with wind action influences the magnitude of waves, and by local topographical morphology. For example, a short-term wave-cut abrasion on a plunging cliff could produce a slight incision observable in a slope failure feature (1 to 3 m high). We refer to this kind of slight pronounced abrasion feature with the term ‘abrasion terrace’. Abrasion platforms on overflow sill ridges represent important additional geomorphic paleo-shoreline markers which are likely produced by the mixing of wave abrasion and traction current action in the overflow direction.

Because of the homogeneous composition of the basaltic stratoid series layers, vertical differential erosion is reduced. Consequently, shore platforms as described in Bird (2008) are almost absent across the Abhe basin. The great number of normal faults which characterize the Tendaho-Gobaad semi-graben could highly affect the recognition and the preservation of continuous morphologic elements of paleo-shorelines. For this reason, during surveys, sites with clear structural patterns were preferred over sites where faulting has probably been involved in sedimentary/erosion dynamics.

The high extensional deformation kinematics of the Tendaho-Gobaad semi-graben do not constitute the only obstacle to abrasion platform recognition. The Late Holocene to current hyper-arid environmental conditions in the Central Afar region, which combine high silicate weathering, wind action, thermoclastism and pronounced slope erosion due to soil/vegetation cover denudation, can also deform the original abrasion features. For this reason, coupling the study of wave-cut and abrasion platforms with supplementary geomorphic and morpho-sedimentary markers is needed for the definition of paleo-shorelines.

4.1.2 – Flat-pebble/cobble beaches

Beach ridges, with their related clastic components, are commonly used as large-scale wave-related geomorphic shoreline features (Hesp, 2006). Across tropical Africa, these continuous, mound-shaped, and linear accumulations of clastic sediments parallel to coastlines are widely used as markers of regressive paleo-shorelines at the end of the AHP (Garcin et al., 2012; Forman et al., 2014; Schuster and Nutz, 2018). In the Central Afar region, beach ridge features are sporadic due to the adverse climatic conditions which prevent their preservation. The total absence of vegetation and soil cover on the basin margins can induce high-energy rill erosion during the short-lived summer rainfalls, causing the vertical displacement of beach ridge clastic components. In addition, heavy silicate weathering and enhanced thermoclastism can produce a high amount of fresh detrital material both from outcrops and from inherited littoral clastic material even on gentle sub-horizontal slope contexts. This pronounced formation process of *in situ* clastic material can lead to some uncertainty in the recognition of continuous ancient beach ridges. Thus, only the coarser components, namely isolated and continuous beach ridges, were considered as paleo-shoreline markers (Sup. Mat. A). Flat-pebble/cobble beaches are often associated with wave-cut and/or abrasion platform surfaces confirming the pertinence of these clastic geomorphic elements as wave-related shoreline features across the Lake Abhe basin.

In this study, the majority of the paleo-shore/foreshore zones are defined by the detection of pebble (4-64 mm diameter) and cobble (64-256 mm diameter; Bird, 2008) concentration bands (Sup. Mat. A).

These can be found as occasional (a few meters long), intermittent or continuous bands. The roundness, flat morphology and smooth surface of clasts allow them to be distinguished from fluvial or slope detrital material. Often, identification of the mineralogical cortege allows us to differentiate local beach clastic products from allochthonous fluvial assemblages. Indeed, some beaches supplied with the mineralogical assemblage of the Awash River were documented (see section 4.2, WK site). The width of the pebble/cobble concentration bands ranges between 2 and 30 meters, and their upper limit is considered a paleo-shoreline elevation marker.

4.1.3 – Gilbert-type deltas and foreshore morphologies

Deltas are shore-related morpho-sedimentary features. Their evolution thus directly reflects changes in water level. In particular, Gilbert-type deltas (first described by Gilbert, 1885) are widely considered to be sensitive recorders of short-term water-level changes (Massari and Colella, 1988; Colella and Prior, 1990; Breda et al., 2007; Gobo et al., 2014, 2015). The distinctive tripartite architecture permits their formation context to be recognized: the subhorizontal bottomset corresponds to the prodelta formation processes, the inclined foreset indicates a subaqueous delta-slope progradation, while the horizontal topset suggests a mouth-bar (fluvial) or slack-water deposition context (Smith and Jol, 1997; Bridge, 2003).

Across the Abhe basin, the Gilbert-type delta is a recurrent landform developed at the mouth of feeder canyons or at the distal end of dejection cones along the basin margins (Fig 3d). Gilbert-type delta facies are generally well-defined and easily recognized (Fig 3e). These peculiar characteristics allow us to easily recognize this kind of paleo-shoreline morphology preserved in the landscape at distinct elevations. The majority of the tributaries of the lower Awash valley are characterized by a high-energy regime due to the high altitudinal gradient between the marginal horsts and the axial alluvial plain. This gradient is at the origin of the formation processes which give deltas a well-defined shape during lake-level highstands: a pronounced slope failure and well-sorted clastic material between the feeder mouth and the delta topset (Fig 3d).

In the EARS lakes, deltas are the combined product of fluvial and wave influences (Schuster and Nutz, 2018). Their shape evolution is driven by wave-induced erosion, and by transport and deposition of river-derived sediment (Anthony, 2015). In the Abhe basin, wave action on delta landforms is evidenced by the frequent association of a flat delta apex associated with abrasion platforms (Fig 3d). The specific description of each Gilbert-type delta facies used as a paleo-shoreline marker in this study is provided in the description of the surveyed sites (section 4.2).

4.2 –A detailed record of the Holocene paleo-shorelines of Abhe basin

4.2.1 – Description of the surveyed sites

Sixteen sites, presenting an assemblage of geomorphic feature types described in section 4.1, were selected from the survey dataset and are summarized in this section. The spatial location of these sites is provided in Fig 4a, while a detailed documentation of each surveyed site is provided in Sup. Mat. A (specific site map, photos, and topographic profiles with the location of the inventoried geomorphic markers). Our results demonstrate the existence of multiple paleo-shoreline sequences from 300 to 420 m a.s.l., which are summarized in Fig 4b. Here, we summarize the characteristics of the paleo-shorelines recognized at the 16 surveyed sites, which we present in alphabetic order.

The AFBO site (‘Afambo’; Sup. Mat. A .2) is a thin ridge located on the foot wall of the stratoid series which separates the Gamari and Afambo lake waterbodies. Survey profiles were carried out on the S-W flank of the hill and on a headland crest that drops into Afambo Lake. Two well pronounced sub-horizontal abrasion platforms associated with beach pebble concentrations were recognized at 399 and 380 m a.s.l. A stromatolitic cover was observed at 370 m a.s.l.

The ALEK site ('Ara le Koma'; Sup. Mat. A .3) is located on a fault scarp on the south ridge of the Gobaad valley. Two paleo-shoreline levels were recognized: the upper one (402 m a.s.l.) is characterized by a sorted line of beach clastic material (cobbles), which likely forms a beach ridge; the lower (389 m a.s.l.) is clearly marked by a well-developed abrasion platform on lacustrine deposits, and by a beach ridge feature composed of cobbles and sub-rounded blocks. Additionally, one stromatolitic level was documented at 441 m a.s.l., and a second stromatolitic cover at 385 m a.s.l.

The AYSO site ('Aysilo'; Sup. Mat. A .4) is located on the northern flank of the Gobaad valley as a foot wall plateau mainly composed of acidic volcanism products (rhyolitic flows and ejecta) which are intercalated in the stratoid series. Three main paleo-shorelines were recognized. The upper level, at 411 m a.s.l., takes the form of a Gilbert-delta apex deposit associated with an overlying sub-horizontal and well-developed wave-cut platform. The median level is void of any clear upper foreshore geomorphic markers (wave-cut features), however a beach pebble concentration band at 382 m a.s.l. indicates a paleo-shoreline level overlying this elevation. A thick and wide stromatolite cover combined with reworked littoral lacustrine material (379 m a.s.l.) is probably associated with the medial paleo-shoreline level. The lower paleo-shoreline level is characterized by a wave-cut abrasion terrace and by abundant beach pebble/cobble concentration lines at 332 m a.s.l. A thin littoral carbonate crust line (microbialite) at 327 m a.s.l. is clearly associated with the lower paleo-shoreline of the AYSO site.

The BE site ('Borawli East'; Sup. Mat. A.5) is situated on the east flank of the Borawli rhyolitic volcano. The BE surveyed profile crosses the limit between the rhyolitic flows and the stratoid series, in which an elevated sedimentary flat-fan deposit formed (as a plateau). It is delimited by the rhyolitic slopes in the west, north and south, and by a basaltic rampart in the east. The basin is supplied by the mountain's detrital load through two feeder canyons and is drained by two dejection channels towards the plain. The sub-horizontal shape of the fan against the steep mountain slopes suggests a Gilbert-type delta morphology. This hypothesis is confirmed by the horizontal topset layers observed at the medial-proximal part of the fan and by the horizontal shape of the fan apex. Thus, we consider the proximal-apex part of the deltaic fan as a marker of an ancient foreshore-line located at 420 m a.s.l. In addition, delta sediments are heavily incised by the current lateral streams which enable the sequence to be easily observed and suggest a post-lacustrine torrential and erosive transport regime, indicating a drop in the water level from the top to the base of the basin, thus confirming our interpretations. Finally, at the BE site, a wave-cut abrasion terrace is documented on the eastern stratoid fault scarp at 402 m a.s.l., which is clearly associated with a stromatolitic cover-line at 400 m a.s.l.

The BSW site ('Borawli South-West'; Sup. Mat. A.6), like the BE site, benefits from reduced structural faults, which favored the detection of morphologic features. Additionally, the rhyolitic and ignimbritic outcrops of the southwest flank of Borawli Mountain provide more pronounced wave erosion features (see Section 4.1.1). For this reason, we counted several well-developed paleo-shorelines at this site. At 415 m a.s.l. some beach cobbles were observed without any clear upper-shore morphologic marker. At 398 m a.s.l., well-developed wave-cut notches and abrasion platforms indicate an ancient shoreline. A few meters below (393 m a.s.l.) a concentration-line of beach cobbles associated with an abrasion platform could belong to the low foreshore zone of the overlying paleo-shoreline or indicate an additional paleolake level. Downward, several wave-cut notches associated with abundant beach pebbles/cobbles and large and well-developed abrasion platforms indicate a series of paleo-shorelines at 387, 381, 372 and 367 m a.s.l. Only one stromatolite level is documented, at 354 m a.s.l.

The BW site ('Borawli West'; Sup. Mat. A.7) is characterized by well-preserved Gilbert-type delta deposits located on the west flank of Borawli Mountain (Fig 3d). At 391 m a.s.l. a sub-horizontal delta apex, associated with an abrasion terrace feature, indicates a paleo-shoreline at this level. On the delta section, the offshore-transition is clearly observable from fine lacustrine deposits, through the bottomset layers to the foreset progradation (Fig 3e), suggesting that these deposits and the related paleo-shoreline were probably developed following a regression from the earlier higher lake level. A lower level was also located at 379 m a.s.l., in the form of a well-developed wave-cut abrasion platform on nearshore sediments.

The DDa site ('Deversoir Djibouti A'; Sup. Mat. A.8) is located along the first part of the southern overflow sill channel of the Abhe basin, which drained the lake water towards the Hanle basin (Fig 1c, 4a). Along the sill, only abrasion platform features were documented, probably due to the high energy of the drainage that occurred through the channel. This is confirmed by the thick fan deposit composed of coarse sediments located at its mouth. Four overflow abrasion terraces were detected on the flanks, at 403, 392, 385, and 380 m a.s.l.

The DSa site ('Deversoir Serdo A'; Sup. Mat. A.9) corresponds to the proximal part of the northern overflow sill of the Abhe basin, which drained the lake water towards the Hanle basin (Fig 1c, 4a). The first and the second part of the sill is intercalated by a small alluvial plain. This sill is higher in elevation than the DDa sill, thus it potentially records only the more ancient and higher drainage phases of the paleolake highstands. Our results confirm this hypothesis with the recognition of two overflow abrasion platforms at 419 and 397 m a.s.l.

The DSb site ('Deversoir Serdo B'; Sup. Mat. 10) is located at the beginning of the distal part of the northern overflow sill of the Lake Abhe basin (Fig 1c, 4a). The overflow channel is not exploitable for paleo-shoreline reconstruction because of the crossing of several faults. However, at the canyon entrance, three paleo-shorelines were documented: the first (403 m a.s.l.) characterized by a well-developed abrasion platform on the stratoid outcrops associated with abundant beach cobbles/pebbles, and the lower two (390, 387 m a.s.l.) characterized by a well-developed abrasion platform on previous lacustrine sediments associated with beach cobbles/pebbles (Fig 3c).

The GTU-AFI site ("Goma'tu-Afa'si"; Sup. Mat. A.11) is the only site surveyed on the western scarp of the Tendaho-Gobaad graben that provided some paleo-shoreline geomorphic information. The limited data are a result of difficult access to the Magenta massif zone. Nevertheless, two paleo-shorelines were documented. The upper one, recognized at 381 m a.s.l. by some beach ridges and the lower, recognized at 371 m a.s.l. by a large wave-cut abrasion platform on lacustrine sediments. One oncolite level is observed at 369 m a.s.l.

The LAK site ('Lakora'; Sup. Mat. A.12) corresponds to the northern extension of the Borawli massif: a large plateau composed of basaltic stratoid series and crossed by few northwest/southeast faults. One paleo-shoreline level was detected at 385 m a.s.l. in the form of an abrasion platform underlined by a beach pebble concentration (383 m a.s.l.). This site is distinguished by a large stromatolitic shelf positioned on the Lakora plateau and ranging between 376 and 372 m a.s.l.

The MN site ('Manda North'; Sup. Mat. A.13) is located on the eastern fault scarps of the Abhe basin, on well-defined northwest/southeast faults. This site is distinguished by the continuity of a well-developed wave-cut abrasion platform located at 385 m a.s.l. and extending over more than 10 km. This shoreline platform is clearly discernable from the faults because it is incised on previous sedimentary deposits placed on the scarp margin. A stromatolitic dome level ranging between 380 and 377 m a.s.l. is likely associated with the shoreline level, while a thin and sporadic littoral carbonate crust (microbialite) was detected at 417 m a.s.l.

The MYTA site ('Mokoyta'; Sup. Mat. A.14) is located on the northern side of the Gobaad valley and is characterized by a stromatolitic cover level at 376 m a.s.l., while no clear paleo-shoreline was detected. A continuous platform surface is located on topographic profiles around 420 m a.s.l., but no other littoral markers were observed.

The RSO site ('Raso'; Sup. Mat. A.15) corresponds to a semi-enclosed basin delimited by northwest/southeast oriented foot-wall basaltic outcrops, located at the eastern margin of the Abhe basin axial valley. This site is distinguished by a gulf or semi-enclosed bay paleo-morphology, where onshore winds would have maintained stable high-water levels producing well-developed littoral geomorphic markers (Bird, 2008). These favorable morphological factors, coupled with systematic field survey allowed us to recognize multiple ancient paleolake levels. Well-defined wave-cut abrasion platforms combined with beach pebble assemblages observed both on the east and west margins of the semi-enclosed bay indicate paleo-shorelines at 419, 410, 403, 393, 389 and 384 m a.s.l. The lower level (384 m a.s.l.) is clearly associated with a thin stromatolitic line located at the same elevation, while two other stromatolitic levels were detected westward at 382 and 376 m a.s.l.

The SD site ('Serdo'; Sup. Mat. A.16) is the northernmost surveyed area which provided some littoral geomorphic markers. The extended plain areas in the north of the basin, which range between 380 and 370 m a.s.l., would have produced large foreshore and shoreline geomorphic markers, making it more difficult to recognize paleo-shore limits. However, in the Serdo area, in the northeastern part of the basin, a continuous abrasion platform and a beach pebble ridge permit the definition of two paleo-shorelines at 400 and 389 m a.s.l.

The SHEK site ('Shekaito Koma'; Sup. Mat. A.17) is located on a small basaltic stratoid outcrop at the center of the Abhe basin. Several paleo-shorelines were documented at the surveyed site, which offered the same morphological advantages of a semi-enclosed basin as described for the RSO site. The highest level at 418 m a.s.l. is marked by abundant beach pebble/cobble concentrations belonging to the paleo-shore/foreshore zone. The underlying levels were detected thanks to abundant clastic beach components and well-developed abrasion platforms at 411, 399, 380 and 369 m a.s.l. The platform at 380 m is incised in foreshore deposits. One stromatolitic line was observed between 369 and 365 m a.s.l.

The WK site ('Wedelli Koma'; Sup. Mat. A.18) is located in the Det Bahari plain on the right bank of the Awash River. It is represented by a hill composed of Tertiary deposits. A wave cut abrasion platform at 418 m a.s.l. is well developed on these deposits and is associated with a large amount of pebbles which indicate an allochthonous origin. The allochthonous mineralogical assemblage could be part of an ancient (Plio-Pleistocene) delta of the Awash River developed at the entrance of the Abhe basin, not far from WK.

4.2.2 – Synthesis of the Abhe basin paleo-shoreline sequence

A synthesis of results from more than one hundred geomorphic shoreline markers has allowed us to define the characteristics and elevations of the main Holocene lake highstands (Fig 4b). First, we defined the Maximum Holocene Highstand Shoreline (MHHS), corresponding to the maximum elevation of well-pronounced geomorphic features recognized in each surveyed site. The MHHS elevations are similar in the central and eastern part of the basin and range between 420 m a.s.l. (central-northern basin) and 410 m a.s.l. (Gobaad basin branch, AYSO site). Secondly, we defined other main paleo-shorelines at 403-400, 385-380, 368 and 330 m a.s.l. (Fig 4b, 7b). These levels are intercalated by minor intermediate levels probably corresponding to lacustrine regression steps.

4.3 – The Lake Abhe stromatolites

Stromatolite structures are the result of the bioaccumulation and precipitation of micritic/sparitic beds from cyanobacteria microbial activity (Casanova, 1991). They are the most used datable markers of lacustrine paleo-shorelines in Eastern Africa (Gasse, 1977; Gasse and Street, 1978; Gillespie et al., 1983; Hillaire-Marcel et al., 1986; Casanova, 1987; Cohen et al., 1997; Garcin et al., 2012). Their structure, mineralogy and isotopic composition provide precise information about their littoral depositional environment, chemical paleo-conditions of the waters, and paleo-hydrological variations (Abell et al., 1982; Casanova and Hillaire-Marcel, 1992; Ghinassi et al., 2012). In this study we present for the first time the macro-/meso-/micro-structure of stromatolites from Lake Abhe with the aim of defining their ecological zonation (shallow/deep-waters), which combined with their radiocarbon measurements adds crucial information to the age model of Lake Abhe paleo-shorelines.

A preliminary investigation of over fifty stromatolite specimens allows us to define at least two main facies. Facies-A is characterized by a micritic poorly-laminated microstructure, organized in vertical micro-column growing patterns. Between the micro-columns, several vertical-oriented voids are often intercalated, and form a complex porosity network from the base to the top of the stromatolite. These bioherms form a well-defined macro-structure of large, linked domes (Fig 5a) which can extend over a few kilometers (LAK site, Sup. Mat. A.12), while the diameter and the thickness of a single dome can reach 1.5 m and 60 cm, respectively. The multiple dome superimposition and their vertical fissured surface form complex morphologies which are attributable to the cerebroïd-like facies as described by Casanova and Hillaire-Marcel (1992), Casanova and Thouin (1990), and Cohen et al. (1997). The large thickness of the stromatolitic linked-dome macro-structure and their micro-/meso-structure indicates a deep water zonation at ~20 m depth (Cohen et al., 1997).

Facies-B is characterized by a well-developed and continuous laminated micro-structure built of alternating Si-Mg-rich and Ca-rich layers (Fig 5.d). Si-Mg-rich laminations are frequently ripple-shaped over the entire bioherm paleo-surface (Fig 5.c). These stromatolites are a few centimeters thick (max 10 cm) and cover clastic blocks or cobbled surfaces, frequently forming oncolite beds (GTU-AFI site, Sup. Mat. A.11). The wave-ripple facies, the oncolite morphology, as well as their irregular surface, indicate a shallow water environment (Casanova, 1986; Schuster and Nutz, 2018). Taking into account the silicic-ferromagnesian regional bedrock sources, Si-Mg-rich layers suggest an increase of detrital delivery events in the lake basin enhancing flow currents, while Ca-rich layers probably suggest periods of lacustrine-dominant biogenic productivity or the onset of evaporitic processes.

4.4 – Paleo-shoreline age control

During field survey, several stromatolites and near-shore lacustrine carbonate products were inventoried and sampled along the entire Abhe Lake basin. The chronological evolution of lake paleo-shorelines is based on the combination of radiocarbon ages measured on 11 stromatolites of both Facies-A and Facies-B and on 9 new and revised published ages on nearshore deposits (Tab 1; Khalidi et al., 2020). Stromatolites were observed at different altitudes ranging from 420 m to 320 m with a concentration between 380 and 360 m.

Stromatolites located in the elevation range of ~381 to ~375 m a.s.l. (Fig 4b, 7b) are often characterized by a superimposition of the well distinguished Facies A and B: Facies-A as a lower and older stromatolite generation and Facies-B as an upper and younger stromatolite generation (Fig 5b, c). The discontinuity between the two facies is marked by a sharp surface of subaerial exposure often filled by a layer of fine sand which can reach 20 cm in thickness as evidenced at the StrIS site (Stromatolis; Khalidi et al., 2020). This facies separation is even characterized by two chronological groups. The older chronological group ranges in date between ~11.1 and ~8.3 ka cal. BP, and only includes ages from Facies-A (Tab 1; ~20 m water depth), suggesting they are related to the paleo-shorelines located around 400 m a.s.l. The more recent facies ranges in date between ~7.7 and ~4.7 ka cal. BP and includes only ages from Facies-B (Tab 1; 0-2 m water depth), suggesting they are related to wave-induced clastic paleo-shorelines located around 385 m a.s.l.

A third chronological group was located at the Str20 site (~369 m a.s.l.), which is characterized by the superimposition of three stromatolitic layers similar to Facies-A, and lying on a palustrine deposit (Str20-SU6). The lower layer (Str20-SU5; 11125 ± 113 cal. BP) is separated by a stone-line in the middle (Str20-SU4; 10530 ± 64 cal. BP) and the upper (Str20-SU1; 10447 ± 73 cal. BP) layers, suggest the existence of subaerial exposure conditions in between.

~420 m (MN site) and ~330 m (AYSO site) a.s.l. paleo-shorelines (Fig 4b; Sup. Mat. A.3, A.4, A.13) present characteristics similar to Facies-B, and thus likely belong to the shallow waters ecological zone. A stromatolite specimen from ~440 m (ALEK site) was dated to 30534 ± 248 cal. BP, thus belonging to the last Pleistocene lake highstand (Abhe-III; Gasse, 1977).

New and published ages on nearshore deposits (lumachelles, shell-rich deposits, diatomites) follow the stromatolite chronological ranges quite well (Tab 1, Fig 7.a). The published ages also allow for the definition of a lower lake level between 3 and 2.8 ka cal. BP, which corresponds to the paleo-shoreline observed around 330 m a.s.l. (site AYSO; Sup. Mat. A.4). Only three nearshore deposits are located between 440 and 400 m a.s.l., and are dated between 10.4 and 9.8 ka cal. BP. They are probably contemporaneous with the geomorphic features and stromatolites of the MHHS located at 440 and 420 m a.s.l. (Fig 4.b, 7.b). Following these results and the respective dating standard deviations, we suggest that the Holocene age of the MHHS was in the range of 10 ± 2.5 ka BP. The offsets of dated littoral features suggest the effect of subsidence due to tectonic deformation which will be discussed below.

5 – Discussion

5.1 –Holocene tectonic subsidence of the Abhe basin

Because of the large rates of horizontal extension that characterize the Central Afar region and the rifting-related vertical motion at the surface (Manighetti et al., 2001; Doubre et al., 2017), we consider it essential to estimate the potential tectonic impact of Holocene rifting on the Lake Abhe paleo-shoreline sequence before discussing its hydro-climatic relevance. Despite the limited number of available data and dates attesting to vertical slipping of the graben, we attempt to find evidence for variations in the rate of subsidence both in space and time.

In the Gobaad branch of the basin (SE, Fig 6a) the MHHS elevation, previously estimated to have occurred ~10 ka cal. BP (see section 4.4), differs by ~10 m from the northern part of the basin (Fig 4b). Several faults are identified and if the relative vertical gap is due to tectonics, the Holocene fault activity would have corresponded to a mean vertical slipping rate of ~1 mm/yr cumulated for the faults observed in this area. This value is of the same order of magnitude as the vertical slipping rate of the faults in the Central Afar determined from topographic profiles across fans by Manighetti et al. (2001). Over the same period of time, the authors estimated a vertical slipping rate of 1 to 3 mm/yr for faults located in the basins to the north, namely Hanle and Gaggade (Fig 1c). Their measurement along the Gobaad fault agrees with a vertical rate of 0.6 mm/yr for the last 1.8 Ma. However, even if the rate over the last 10 ka period could not be measured, it is probably higher by a factor of 2 or 4, as has been demonstrated for most of the faults in the Central Afar (Manighetti et al., 2001).

In the Logiya-Saha branch of the basin (NW, Fig 6a), we can compare the littoral carbonate samples of the same age (~10.4 ka cal. BP, Gasse_94 and Strom20-SU1; Tab 2; Fig 6), which show an elevation offset of 49.2 m. The sample Gasse_94 is located on the left bank of the Logiya River valley, while Strom20-SU1 was sampled within the Saha plain (Fig 6a, b). Between the sites, several normal faults are dissecting the surface and mainly correspond to the southern end of the active Manda-Hararo volcano-tectonic rift segment (Fig 6; Abbate et al., 1995; Manighetti et al., 2001; Doubre, 2017). The elevation offset is therefore consistent with a mean vertical subsidence rate of 4.7 mm/yr in the central part of the rift with respect to its margin. A high amplitude of subsidence rate is expected in the area, since this rift is affected by regular crustal magma intrusion events within its rift zone, which induce its subsidence as was the case during the last 2005-2010 dyke sequence event (Grandin et al., 2009, 2011).

The vertical offset between the samples Gasse_50 (right bank of the Logiya River valley) and Strom14 (Poz-124783; Magenta ridge; Tab 2), both dated around ~7.7 ka cal. BP, is more complex because they are located ~60 km apart (Fig. 6a). However, these dates suggest a mean differential vertical rate reaching ~9.1 mm/yr over this period. Acocella (2010) mapped the down-sagging of the surface of the Tendaho graben due to the withdrawal of magma from the deep elongated reservoir. This collapse of the surface was particularly important over the period 2 to 0.5 Ma, but may have persevered at a lower rate over the Holocene period. The recent subsidence can be related to the current extension taking place across the graben estimated with GNSS measurements. The rifting across the Tendaho graben occurs with both an opening rate of 7 mm/yr between the southwestern margin of the graben and the Gamari plateau (Fig. 6a, Doubre et al., 2017), and a related subsidence of the central part which is not clearly estimated using a geodetic approach. However, because the Tendaho graben is not considered a very tectonically and magnetically active rift segment, our subsidence rate within the central part of the Tendaho graben (~9.1 mm/yr) is probably overestimated if we compare it to the subsidence rate of the inner floor of the active volcano-tectonic segment of Asal, which reached ~8 mm/yr for the last 6 ka, and 8-9 mm/yr for the last 35 ka (Stein et al., 1991).

All these results show that the Holocene subsidence taking place within the Tendaho graben varies in time and in space. A striking result is that all the MHHS measurements in the central and the northeastern parts of the Tendaho-Gobaad graben are at the same elevation (~420 m) which suggests that most of this area was affected by quite a homogeneous subsidence during the Holocene period (Fig 4). This evidence is confirmed by several stromatolites at the same elevation and age throughout the central and northeastern basin (Tab 1, Fig 7a, 7c), which indicates a maximum vertical displacement of ~5 m between them over the last 5-6 ka. However, our results show a relatively higher subsidence rate (~4.7 mm/yr) in the northern part of the Tendaho graben (Logiya-Saha branch; Fig 6a, 6b) and a lower subsidence rate of ~1 mm/yr in the Gobaad valley (Fig 6a, 6b). This variation in subsidence rate is also consistent with the variations in opening rate measured by GNSS across both ends of the graben (Doubre et al., 2017). This is also consistent with the model proposed by Tapponnier et al. (1990) and Manighetti et al. (2001, 1998) where the Tendaho graben corresponds to the tip of the Red Sea ridge propagating southeastward into the Afar, and overlapping with the Aden Ridge. The opening and related subsidence rates are larger in the northwest than the southeast, near Lake Abhe (Fig 6a), where the lack of evidence of active deformation matches with smaller vertical displacements.

In light of these results, the low subsidence rates cannot support the hypothesis of a tectonic-driven lacustrine transgression between the Early and the Middle Holocene, since a subsidence rate of the basin that is larger than the 'evaporation rate' cannot be envisaged.

Taking into account the paleo-shoreline elevation offsets due to the tectonic vertical slipping between the SW graben margin and the central/NE basin (Fig. 6a), we can correct the elevation of samples with the aim of producing a more accurate Holocene lake-level fluctuation model. We consider the subsidence rate measured along the Logiya-Saha transect reliable, and have therefore calibrated elevations of samples from the SW ridge of the basin (see Tab 1).

5.2 - The last 11 ka of Abhe Lake fluctuations and their hydro-climatic relevance

On the basis of the documentation of 107 littoral geomorphic features and their chronological control obtained from 53 ^{14}C ages on shallow-/deep-water stromatolites and nearshore deposits, we propose a robust Holocene water-level reconstruction model of Lake Abhe. The lake-level variation curve takes paleo-shoreline tectonic deformations into account thanks to the offset correction calculated from Holocene subsidence rates, which are estimated from stromatolite and paleo-shoreline ages. In addition, the integration of archaeological excavation datasets from lake-side prehistoric occupations

(Khalidi et al., 2020) enables us to add an altitudinal control to lake-level reconstructions that improves the paleo-hydrological model and constrains some reservoir age effect anomalies (Fig 7a).

After the hyperarid episode coinciding with the Younger Dryas cooling event (Garcin et al., 2007; Gasse et al., 2008), the first evidence for lake-level rise in the Holocene is dated on a stromatolite to ~11.1 ka cal. BP (Strom20-SU5), after which the Maximal Holocene Highstand Shoreline (MHHS, ~420 m a.s.l.) reached its peak sometime around 10 ka BP. Following a probable water-level stabilization at ~400 m a.s.l., dated between ~9.8 and ~8.8 ka cal. BP, the lake level regressed slowly to ~375 m a.s.l. until ~8.3 ka cal. BP and abruptly dropped to ~250 m a.s.l. at ~8 ka cal. BP. This Early Holocene transgression (between ~11.1 and 8.3 ka cal. BP) generally corresponds to the Abhe-IV lacustrine phase defined by Gasse (1977). During this phase the overflow sills were certainly active, as evidenced by the DDa, DSa and DSb sites (see 4.2.1 and Sup. Mat. A.8, A.9, A.10).

The resurgence of Mid-Holocene humid conditions as revealed by paleo-shoreline markers was recorded at ~7.7 ka cal. BP. The lake reached the highest Mid-Holocene water level between ~6 and ~5.6 ka cal. BP (~380-385 m a.s.l.). This lacustrine transgression corresponds to the Abhe-IV lacustrine phase defined by Gasse (1977). After a slow lowering of the waterbody between ~5.6 and ~4.6 ka cal. BP, the absence of littoral deposits at lower elevation suggests a drastic and rapid drop in level. Finally, the lake rose gently from 2.8 ka cal. BP until it reached its maximal Late Holocene level (330 m a.s.l.) at ~1.5 ka cal. BP.

Lake-level variations are generally attributed to changes in monsoon precipitation conditions over the catchment area (i.e., the Ethiopian Highlands; Gasse, 1977). Paleoclimatic interpretation of lake-level changes are rightly based on the analysis and modeling of the hydrological precipitation and evaporation balance (Junginger and Trauth, 2013) coupled with paleolimnological studies. However, changes in lake level and sedimentation can be affected by local geomorphic factors which can mitigate the climatic signal, leading to an underestimation or overestimation of the modeled data. The 420, 400 and 385 m a.s.l. Lake Abhe highstands (Fig 7b) are considered to be precipitation-induced lake fillings from Ethiopian Highland summer rainfalls, regulated by overflows towards the Hanle basin

(Fig 1c, 6, 7a). We observe several regression steps over the course of the Holocene that were the result of incision of the overflow sills and subsequent water-level stabilizations, and which are demonstrated by the multi-level abrasion platform sequences documented at the DDa and DSa/DSb overflow sites (see 4.2.1 and Sup. Mat. A.8, A.9, A.10). Consequently, the MHHS doesn't directly imply the highest precipitation or water inflow period of the Holocene, because was regulated by these incision processes. However, in future studies, the estimation of the sill overflow incision rates could provide an additional parameter for the calculation of hydro-balance models with the aim to give precise water inflow or precipitation rates from the Awash River catchment.

Holocene changes in water level are not always the result of balanced source-to-sink mechanisms. A non-linear response of the hydrological system could be conditioned by the interconnections between basin catchments. During the Early/Middle Holocene, the Awash River catchment area was temporarily supplied by freshwater inputs from adjacent basins (Fig 8d). The Ziway-Shala paleolake overflow towards the Awash catchment was demonstrated for the first time by Nilsson (1940) at 1670 m a.s.l., and later revised by Grove and Goudie (1971), Gasse and Street (1978) and Gillespie et al. (1983; Fig 8c). The possible transient fluvial connection to the Awash River is in phase with the beginning of the Early Holocene Lake Abhe highstand, coinciding with the maximal solar irradiation at 10° N around 11 ka cal. BP (Fig 8b, c). Similarly, the Mid-Holocene maximal Abhe Lake level, which occurred between 6 and 5.6 ka cal. BP, is in phase with the observed Mid-Holocene Ziway-Shala Lake overflow, which could have made a significant contribution to the Lake Abhe water-level balance. The Holocene connectivity between these two basins is even supported by the apparition of the *Cyprinidae sp.* fish in the Lake Abhe basin around ~10 ka BP probably introduced from the Ziway-Shala basin where it was attested since 13 ka BP (Coudert, 2019). Additionally, Sagri et al. (2008) demonstrated that during the Early Holocene, the Awash River contributed to the water filling of the Ziway-Shala Basin, confirming the mutual interconnection between these two basins.

After excluding the possibility of tectonic-induced Holocene lake transgressions (sec 4.2) and providing some elements that demonstrate the primary local geomorphic control of lacustrine fluctuations (overflow sill incision), we can consider the Holocene Abhe lake-level reconstruction as a reliable record of monsoon-induced hydrologic changes over the Awash basin.

5.3 – Implications for Holocene East African moisture mass dynamics

Thanks to Lake Abhe's geographic position, located in the northern EARS extremity (Fig 1a), our results add new elements to the discussion of the timing of the AHP transitions in Eastern Africa and more particularly across the EARS basins.

We compared our results with other southernmost lacustrine basins along the rift axis at latitudes between 12° N and the Equator, with the aim of studying Holocene hydrological feedback across a coarse N-S transect (Fig 10). From north to south, we included lake-level paleo-data from Abhe (11°-12° N; this study; Fig 9c), Ziway-Shala (7.5°-8.5° N; Gillespie et al., 1983; calibrated to calendar age; Fig 9d), Suguta (1.5°-2.5° N, Garcin et al., 2009; Junginger and Trauth, 2013; Fig 9e) and Nakuru basins (0.5° N; Richardson and Dussinger, 1986; calibrated to calendar age; Fig 9f). With the aim to constrain the hydro-climatic significance of these water-level changes, we added δD_{wax} data - considered a proxy for precipitation/air-mass dynamics – from the northern and southern extremities of the investigated area (Tana Lake, 11.5°-12.5° N, Costa et al., 2014; Challa Lake, 3°S, Tierney et al., 2011; Fig 9a, 9g).

Our results show a resurgence of humid conditions after the YD cooling event of the Northern Hemisphere (Younger Dryas; Alley, 2000; Rasmussen et al., 2014) around ~11.1 ka cal. BP and a reduction of the high Early Holocene hydrological regime from ~8.7 ka cal. BP. A shift and reduction in hydrographic regimes as early as ~8.7 ka cal. BP has already been pointed out by recent studies, and interpreted as a consequence of changes in monsoonal dynamics over the Ethiopian Highlands (Blanchet et al., 2014; Ménot et al., 2020; Mologni et al., 2020). Despite a possible chronological incertitude of the compared records, a northward installation of Mid-to-Late Holocene aridification with a ~1000 yr delay with respect to the southern EARS basins can be suggested (Fig 9).

Indeed, the observed time-latitude delays of the Mid-to-Late Holocene aridification events are in conflict with the ITCZ oscillation processes: Mid-Holocene ITCZ southward migration should correspond to a southward aridification, while we observe the contrary (Fig 9). However, changes in precipitation are not only the result of atmospheric convection over the rain belt, but could have also been produced by the migration of other convergence zones.

As proposed by (Hailemichael et al., 2002), and later by Tierney et al. (2011) and Junginger et al. (2014), the incursion of the Congo Air Boundary (CAB) in the specific morpho-tectonic context of the EARS water-sources would have contributed additional moisture to persistent humid conditions, in contrast to the Mid-Holocene southern migration of the ITCZ. This process would have been the result of a high pressure gradient between the CAB and the Indian Summer Monsoon (ISM) air masses, which enhanced the influence of the West African Summer Monsoon (WAM) over Northeast Africa (Camberlin, 1997; Marzin and Braconnot, 2009; Junginger et al., 2014). Similarly, the intensified summer Indian monsoon of the Early Holocene can be hypothesized to have pulled both components of the Ethiopian monsoon eastward (Overpeck et al., 1996). The same hypothesis has been advanced to explain the lower and prolonged leaf-wax values at Tana Lake during the Mid-Holocene period (Costa et al., 2014; Fig 10b). The intensified ISM favored an east-shifting of the CAB, fueling humid conditions over the Ethiopian Highlands. In this scenario, thanks to its Eastern Ethiopian Highland sources, Lake Abhe's hydrology would have been particularly subjected to the CAB moisture mass influences from the beginning to the end of the AHP. In contrast, Challa Lake, which lies beyond the CAB boundary (Fig 10; Tierney et al., 2011), presents a short Holocene humid regime and follows the subsequent progressive southern retreat of the rain belt (Fig 9g).

In summary, the persistence of ISM-CAB pressure regulation combined with the geomorphic patterns of the EARS, enhanced the influence of the CAB moisture in the northeast African Rift until the end of the AHP producing a progressive northward development of the arid Mid-Holocene conditions across the EARS (Fig 10). These patterns show an inverse air-moisture dynamic compared with Central and

Western intertropical Africa, where the development of Middle-Holocene arid conditions followed the progressive southward retreat of the ITCZ (Shanahan et al., 2015; Fig 9h).

6 – Conclusion

The documentation, interpretation and dating of more than one hundred littoral geomorphic features have permitted the reconstruction of a detailed paleo-shoreline sequence that elucidates the Holocene lake-level rise and fall of the widest lacustrine system in the Afar region, Lake Abhe.

We observe that after the Younger Dryas arid event (~12.9 to ~11.7 ka) Lake Abhe began to rise around 11.1 ka cal. BP peaking at ~9.8 ka cal. BP, in phase with the maximum insolation values over the tropics. A gradual decrease in lake level is recorded from ~9 ka cal. BP until a drastic drop in level occurred at ~8 ka cal. BP. A resurgence of humid conditions is confirmed from ~7.7 ka BP with the establishment of a stable lake highstand until ~4.6 ka cal. BP when the large waterbody was definitively reduced by a prominent desertification process in the Afar region. Nonetheless, during the Late Holocene, a minor lake transgression was recorded between ~2.4 and ~1.4 ka cal. BP, followed by a lake lowstand which persists until the present day.

The documentation of multiphase sill overflow incisions towards the adjacent Hanle basin demonstrates geomorphic control on Holocene highstand elevations. In addition, new ages on carbonate littoral material allow us to propose a Holocene subsidence rate of the northern Tendaho-Gobaad graben.

Past Lake Abhe level fluctuations are thus the result of combined monsoonal dynamics concentrated in the Ethiopian Highlands (Viste and Sorteberg, 2013) and local earth surface processes. While long-term hydrological changes are mainly triggered by orbitally-driven insolation pacing, our results suggest that short-term events, as well as the variability of humid/arid period durations, may be related to internal/regional climatic and geomorphic forcing mechanisms which are not yet fully understood.

Comparison of our results with other lacustrine archives indicates a northward Mid-Holocene aridification along the EARS, which disagrees with the classic scenario of the ITCZ southern retreat as a possible cause of the southern Mid-Holocene aridification over Africa. This evidence could be explained by the incursion of air moisture masses in the EARS induced by a high pressure gradient that formed between the Congo Air Boundary and the Indian Summer Monsoon air masses, resulting in enhanced precipitation over Northeastern Africa. These conditions would have supported the persistence of large waterbodies and their related eco- and anthropo-systems in the northern EARS lowlands until ~4.6 ka cal. BP.

Acknowledgments

The fieldwork and analyses presented were carried out in the framework of the Volcanological and Archaeological Program for Obsidian Research-Afar (VAPOR-Afar) directed by L. Khalidi and by the PSPCA project directed by J. Cauliez. The VAPOR-Afar project was funded by an American Institute for Yemeni Studies Grant (United States) in 2014 and a Fyssen Foundation “Subvention de Recherche” (France) awarded to LK between 2015 and 2016, partially funded by the CEPAM-CNRS (STEP) and a BQR-OCA in 2019, the ANR 14-CE31-0023 ‘Big Dry’ between 2016 and 2019 and by the TelluS-RIFT-INSU “AGXIM” and the ‘Mission pour les initiatives transverses et interdisciplinaires du CNRS’ (France) awarded to CD between 2017 and 2020. Between 2018 and 2020, this research was supported by the French government, through the UCAJEDI Investments in the Future project managed by the National Research Agency (ANR) with the reference number ANR-15-IDEX-01. The PSPCA project was funded by the French Ministry of European and Foreign Affairs, by the ANR 14-CE31-0023 ‘Big Dry’, the INEE, the Institut des Steppes and the Fyssen Foundation. A Centre Français des Etudes Ethiopiennes (CFEE) fieldwork grant for both field projects was awarded to C. Mologni in 2018. We thank E. Soteras for the aerial photograph of the Stromatolis site (Fig. 5.a) and we are grateful to Catherine Buchanan of the

'Office of International Scientific Visibility' of the University Côte d'Azur for the manuscript revision. Finally, the kind, thorough and constructive comments provided by Y. Garcin and an anonymous reviewer allowed us to significantly improve the quality of this manuscript.

Captions

Fig 1: **a**) Location of the East African Rift System (EARS; red color) and the study area, corresponding to the Abhe Lake basin (red star). Summer position (June) of present African tropical frontal systems: the Intertropical Convergence Zone (ITCZ) and Congo Air Boundary (CAB; Viste and Sorteberg, 2013); and the wind directions of the Western African Summer Monsoon (WAM) and the Indian Summer Monsoon (ISM). **b**) Simplified morpho-tectonic patterns of the Afar Triangle depression (light gray), enclosed by the Arabian, Nubian and Somalian plates (pre-rift groups, dark gray) with the location of the present Lake Abhe (red star). **c**) Structural map of the Afar depression (modified from Doubre et al., 2017 in which the present Abhe Lake (red star), the extension of the Abhe Lake sedimentary system (light green), other Central Afar sedimentary basins (light yellow), the present natural waterbodies (blue), the ancient Abhe basin overflow sills (blue arrows), recent lava flows (light red), active (red lines) and ancient (dashed red lines) rift segments (modified from Barberi and Varet, 1972) are indicated. The dashed dark green line indicates the Tendaho-Gobaad discontinuity, while the large and small faults are indicated by bold and thin lines, respectively.

Fig 2: Graphic comparison between littoral geomorphic feature elevations measured with the GEO7x differential GPS in the field (red triangles) and the same GPS point elevations processed with a TanDEMx (12.5 m; green dots) and SRTM (30 m; black squares).

Fig 3: Selected photographs of the surveyed littoral geomorphic features described. **a**) Well-developed wave abrasion notches combined with abrasion platform and beach pebble/cobble concentration features at the BSW site (Sup. Mat. A.). **b**) Ridge made on the foot wall of the basalt stratoid series which separates the Gamari and Afambo lake waterbodies with a well-developed seaward-sloping shore morphology (Sunamura, 1992) and the location of the relative paleo-shoreline (dashed black line) at the Afbo site (Sup. Mat. A.2). **c**) Well-developed abrasion platforms on basaltic bedrock and on sediments at the DSb site (Sup.Mat. A.). **d**) Gilbert-type delta morphology at the BE site with black arrows indicating: the feeder canyon, the apex delta and the connected abrasion platform (Sup. Mat. A.). **e**) Gilbert-type delta facies at the BE site (Sup. Mat. A.).

Fig 4: Digital Elevation Model of the Central Afar Region base map (SRTM) with the **a**) location map of surveyed sites over the Abhe Lake basin (black line squares) showing the Maximal Holocene Highstand Shoreline (MHHS, 420 m a.s.l.; white line), location of the ancient overflow sills (black arrows) and the Hanle basin. **b**) presented from the western to the eastern side of the Abhe Lake basin, a synthesis of the surveyed sites showing the MHHS (bold and dotted blue lines), the paleo-shorelines (black arrows), the stromatolite deposits (bold red lines) and corresponding calibrated median ^{14}C ages (red text). The dashed black lines indicate the main paleo-shorelines while the dashed red line indicates the connection between stromatolites with similar calendar ages.

Fig 5: Selected macro-/meso-/micro-photographs of the Lake Abhe stromatolites. **a**) Aerial photo of the StrIS site showing the macro-structure of connected large stromatolitic domes, the sampling zone of the sample Strom31 (Poz-113925; Tab 1) and the location of the Stromatolis archaeological site (Khalidi et al., 2020), where the dated Stromatolis-SU1 (Poz-113841) was sampled (Tab 1). Photo courtesy of E. Soteras **b**) Photograph showing the superimposition of stromatolitic Facies-A and -B at the site LAK (Sup. Mat. A.). **c)** Photograph of a polished section of a stromatolite (Strom_11) showing the meso-structure superimposition of stromatolitic Facies-A and -B. **d**) SEM-EDX analysis mapping showing the Si-Mg concentration in the stromatolite Facies-B rippled laminations.

Fig 6: **a**) Digital Elevation Model of the Central Afar Region (SRTM) showing the current horizontal velocities with respect to the stable Nubian plate deduced from GNSS field measurements (black dashed arrows; after Doubre at al. 2017), the location of samples used for the calculation of the subsidence rate (black arrows, this study), the MHHS (red line), the location of the ancient overflow sills (blue arrows), of new (green dots) and published (red dots) dated nearshore deposits, of the stromatolitic deposits (blue triangles), the topographic profile represented in Fig. 6b (black line, A-A'), and the littoral geomorphic features (yellow dots) inventoried during the survey. **b)** Topographic profile A-A' with the main graben faults, and with the location of samples used for the calculation of the subsidence rate (black arrows, this study) and relative offset (red text).

Fig 7: Holocene Abhe Lake -level reconstitution. **a**) Curve of Abhe Lake -level fluctuations (black line) showing the main lake highstands (light blue squares), the dated Facies-A (blue triangles), Facies-B (inverted blue triangles) and undetermined facies (empty blue triangle) stromatolites, the new (black squares) and published (black dots) dated nearshore deposits (Gasse 1975 revised), and the main human prehistoric occupations (empty red rhombuses). **b**) Histogram of the totality of the inventoried paleo-shoreline features (red lines) and stromatolite deposits (blue lines) showing counts against the elevations in ranges of 5 m. **c**) Longitude against elevation graph of the totality of stromatolites inventoried (empty blue triangles) showing the main Holocene Abhe Lake highstand levels (light blue bands).

Fig 8: Holocene interconnectivity between the Ziway-Shala and Awash River catchments. **a**) Paleovariations in June insolation at 10° N (after Berger and Loutre, 1991). **b**) Abhe Lake-level fluctuations (for the legend see Fig 7). **c**) Ziway-Shala Lake-level fluctuations from calibrated ages (after Gillespie et al. 1983). Overflow elevations are indicated with blue lines, while the transient fluvial interconnectivity between the two basin catchments are indicated with light blue bands. **d**) Map of the Ziway-Shala basin and Awash catchment areas (black bold line) showing the Awash River course (bold blue line), the secondary rivers (light blue lines), the present (light blue) and Early-Mid-Holocene (blue) lake surfaces, and the Early-Mid-Holocene overflows (red arrows).

Fig 9: Paleovariations in **a**) June insolation at 10° N (Berger and Loutre, 1991); **b**) δD_{WAX} from Lake Tana (Costa et al., 2014); **c**) water level of Abhe Lake (this study); **d**) human subsistence strategies in the Central Afar region (Khalidi et al., 2020); and water levels of **e**) Ziway-Shala Lake (Gillespie et al., 1983), **f**) Suguta Lake (Junginger and Trauth, 2013) and **g**) Nakuru Lake (Richardson and Dussinger, 1986). Original radiocarbon dates were calibrated and converted into calendar years. Paleovariatons in **h**) δD_{WAX} from Lake Challa (Tierney et al., 2011) and June insolation at the equator (Berger and Loutre, 1991; yellow lines).

Fig 10: East Africa map of monthly precipitation average (mm/month) in June, from the CRU-TS 4.03 dataset (Harris et al., 2014) downscaled with WorldClim 2.1 (Fick and Hijmans, 2017). Blue stars indicate the location of lacustrine basins reported in Fig 9: b – Lake Tana; c – Lake Abhe; e – Ziway-Shala Lake; f – Lake Suguta; g – Lake Nakuru; and h – Lake Challa. Dashed green line indicates the suggested position of the CAB before 8.5 ka cal. BP, while the dashed red lines indicate the position of the CAB and ITCZ after 8.5 ka cal. BP. Black arrows correspond to the air moisture mass direction of the WAM and of the ISM.

Table 1 : New and previous ^{14}C ages calibration and elevation correction: ‡ = Ages on nearshore/offshore deposits; † = ages for reservoir effect estimation; * = Selected and revised ages on nearshore/offshore deposits from Abhe basin, from Gasse (1975), the ID number refers to the sample number indicated in Gasse 1975 and the Lab ID refers to the Laboratory indicated in Gasse 1975 : LGD = Laboratoire de Géologie Dynamique, Paris; LFR = Laboratoire des Faibles Radioactivités CEA-CNRS, Gif-sur-Yvette; GU= Gakushuin University, Tokyo. Str = Stromatolite undetermined; Str-A = stromatolite Facies-A; Str-B = Stromatolite Facies-B; *Mt* = *Melanoides tuberculata*; Ch = Charcoal; hcc = hydrothermal carbonate crust; Sh = Shells mix; U = Unios bivalve shell.

Table2: Subsidence rate calculation table from dated littoral carbonate samples.

References

Abbate, E., Passerini, P., Zan, L., 1995. Strike-slip faults in a rift area: a transect in the Afar Triangle, East Africa. Tectonophysics 241, 67–97. https://doi.org/10.1016/0040-1951(94)00136-W

Abell, P.I., Awramik, S.M., Osborne, R.H., Tomellini, S., 1982. Plio-pleistocene lacustrine stromatolites from lake Turkana, Kenya: Morphology, stratigraphy and stable isotopes. Sedimentary Geology 32, 1–26. https://doi.org/10.1016/0037-0738(82)90011-2

Acocella, V., 2010. Coupling volcanism and tectonics along divergent plate boundaries: Collapsed rifts from central Afar, Ethiopia. Geological Society of America Bulletin 122, 1717–1728. https://doi.org/10.1130/B30105.1

Acton, G.D., Stein, S., Engeln, J.F., 1991. Block rotation and continental extension in Afar: A comparison to oceanic microplate systems. Tectonics 10, 501–526. https://doi.org/10.1029/90TC01792

Alley, R.B., 2000. The Younger Dryas cold interval as viewed from central Greenland. Quaternary science reviews 19, 213–226.

Anthony, E.J., 2015. Wave influence in the construction, shaping and destruction of river deltas: A review. Marine Geology 361, 53–78. https://doi.org/10.1016/j.margeo.2014.12.004

Audin, L., Quidelleur, X., Coulié, E., Courtillot, V., Gilder, S., Manighetti, I., Gillot, P.-Y., Tapponnier, P., Kidane, T., 2004. Palaeomagnetism and K-Ar and ^{40}Ar/^{39}Ar ages in the Ali Sabieh area (Republic of Djibouti and Ethiopia): constraints on the mechanism of Aden ridge propagation into southeastern Afar during the last 10 Myr. Geophysical Journal International 158, 327–345. https://doi.org/10.1111/j.1365-246X.2004.02286.x

Barberi, F., Varet, J., 1977. Volcanism of Afar: Small-scale plate tectonics implications. Geol. Soc. Am. Bull., 88, 1251–1266.

Barberi, F., Varet, J., 1972. Carte géologique de la chaine volcanique de l’Erta Ale (Afar, Ethiopie). Géotechnip.

Berger, A., Loutre, M.F., 1991. Insolation values for the climate of the last 10 million years. Quaternary Science Reviews 10, 297–317. https://doi.org/10.1016/0277-3791(91)90033-Q

Bird, E.C.F., 2008. Coastal geomorphology: an introduction, 2nd ed. ed. Wiley, Chichester, England ; Hoboken, NJ.

Blanchet, Frank, M., Schouten, S., 2014. Asynchronous Changes in Vegetation, Runoff and Erosion in the Nile River Watershed during the Holocene. PLOS ONE 9, e115958. https://doi.org/10.1371/journal.pone.0115958

Boucaurt, M., Clin, M., Pouchan, P., Thibault, C., 1985. Impact des événements tectono-volcaniques Plio-Pléistocenes sur la sédimentation en République de Djibouti (Afar Central). Geologische Rundschau 7, 123–136.

Braconnot, P., Marzin, C., Gregoire, L., Mosquet, E., Marti, O., 2008. Monsoon response to changes in Earth’s orbital parameters: comparisons between simulations of the Eemian and of the Holocene. Clim. Past 14.

Breda, A., Mellere, D., Massari, F., 2007. Facies and processes in a Gilbert-delta-filled incised valley (Pliocene of Ventimiglia, NW Italy). Sedimentary Geology 200, 31–55. https://doi.org/10.1016/j.sedgeo.2007.02.008

Bridge, J.S., 2003. Rivers and Floodplains: Forms, Processes, and Sedimentary Record. Blackwell Publishing, Malden.

Bronk Ramsey, C., 2001. Development of the Radiocarbon Calibration Program. Radiocarbon 43, 355–363. https://doi.org/10.1017/S0033822200038212

Camberlin, P., 1997. Rainfall Anomalies in the Source Region of the Nile and Their Connection with the Indian Summer Monsoon. JOURNAL OF CLIMATE 10, 13.

Casanova, J., 1991. Biosedimentology of Quaternary stromatolites in intertropical Africa. Journal of African Earth Sciences (and the Middle East) 12, 409–415. https://doi.org/10.1016/0899-5362(91)90090-L

Casanova, J., 1987. Stromatolites et hauts niveaux lacustres pléistocènes du bassin Natron-Magadi (Tanzanie-Kenya). Pleistocene stromatolites and high lake levels of the Natron-Magadi basin (Tanzania-Kenya). Sciences Géologiques. Bulletin 40, 135–153. https://doi.org/10.3406/sgeol.1987.1756

Casanova, J., 1986. Les Stromatolites Continentaux: Paleoecologie, paleohydrologie, Paleoclimatologie. Application au Rift Gregory. Université d’Aix-Marseille II.

Casanova, J., Hillaire-Marcel, C., 1992. Chronology and Paleohydrology of Late Quaternary High Lake Levels in the Manyara Basin (Tanzania) from Isotopic Data (“0, 13C, 14C, Th/U) on Fossil Stromatolites. Quaternary Research 38, 205–226.

Casanova, J., Thouin, C., 1990. Biosédimentologie des stromatolites Holocénes du Lac Tanganyika, Burundi. Implications hydrologiques: Bulletin de la Société Géologique de France 4, 647–656.

Clement, A.C., Cane, M.A., Seager, R., 2001. An Orbitally Driven Tropical Source for Abrupt Climate Change. JOURNAL OF CLIMATE 14, 7.

Cohen, A.S., Talbot, M.R., Awramik, S.M., Dettman, D.L., Abell, P., 1997. Lake level and paleoenvironmental history of Lake Tanganyika, Africa, as inferred from late Holocene and modern stromatolites. Geological Society of America Bulletin 18.

Colella, A., Prior, D.B., 1990. Coarse–grained deltas, Int. Assoc. Sedimentol. Spec. Publ.

Collins, J.A., Govin, A., Mulitza, S., Heslop, D., Zabel, M., Hartmann, J., Röhl, U., Wefer, G., 2013. Abrupt shifts of the Sahara–Sahel boundary during Heinrich stadials. Climate of the Past 9, 1181–1191. https://doi.org/10.5194/cp-9-1181-2013

Collins, J.A., Prange, M., Caley, T., Gimeno, L., Beckmann, B., Mulitza, S., Skonieczny, C., Roche, D., Schefuß, E., 2017. Rapid termination of the African Humid Period triggered by northern high-latitude cooling. Nature Communications 8. https://doi.org/10.1038/s41467-017-01454-y

Costa, K., Russell, J., Konecky, B., Lamb, H., 2014. Isotopic reconstruction of the African Humid Period and Congo Air Boundary migration at Lake Tana, Ethiopia. Quaternary Science Reviews 83, 58–67. https://doi.org/10.1016/j.quascirev.2013.10.031

Coudert, L., 2019. La place de la pêche pendant l'Holocène de la vallée du Rift au Sahel occidental. Université de Toulouse 2 Jean Jaurès.

Davies, F.J., Renssen, H., Blaschek, M., Muschitiello, F., 2014. The impact of Sahara desertification on Arctic cooling during the Holocene. Clim. Past Discuss. 10, 1653–1673. https://doi.org/10.5194/cpd-10-1653-2014

deMenocal, P., Ortiz, J., Guilderson, T., Adkins, J., Sarnthein, M., Baker, L., Yarusinsky, M., 2000. Abrupt onset and termination of the African Humid Period: rapid climate responses to gradual insolation forcing. Quaternary Science Reviews 19, 347–361.

Déprez, A., Doubre, C., Masson, F., Ulrich, P., 2013. Seismic and aseismic deformation along the East African Rift System from a reanalysis of the GPS velocity field of Africa. Geophysical Journal International 193, 1353–1369. https://doi.org/10.1093/gji/ggt085

Doubre, C., 2017. TelluS RIFT: Aléas géologiques, histoire du peuplement et transformations socio-économiques d'une zone lacustre au coeur de la dépression Afar (Ethiopie) (Dossier Scientifique). Institut de Physique du Globe de Strasbourg (IPGS, UM7516).

Doubre, C., Déprez, A., Masson, F., Socquet, A., Lewi, E., Grandin, R., Nercessian, A., Ulrich, P., De Chabalier, J.-B., Saad, I., Abayazid, A., Peltzer, G., Delorme, A., Calais, E., Wright, T., 2017. Current deformation in Central Afar and triple junction kinematics deduced from GPS and InSAR measurements. Geophys. J. Int. 208, 936–953. https://doi.org/10.1093/gji/ggw434

Faure, H., Gasse, F., Roubet, C., Taieb, M., 1971. Les formations lacustres Holocènes et l'industrie épipaléolithique de la région de Loggia (bassin du lac Abhé Ethiopie). Presented at the VII Congrès Panafricain de préhistoire et Quaternaire, Addis Abeba, pp. 391–403.

Fick, S.E., Hijmans, R.J., 2017. WorldClim 2: new 1-km spatial resolution climate surfaces for global land areas. Int. J. Climatol 37, 4302–4315. https://doi.org/10.1002/joc.5086

Fontes, J.C., Pouchan, P., 1975. Les cheminées du lac Abhé (T.F.A.I.). C.R. Acad. Sci. Paris 280, 383–386.

Forman, S.L., Wright, D.K., Bloszies, C., 2014. Variations in water level for Lake Turkana in the past 8500 years near Mt. Porr, Kenya and the transition from the African Humid Period to Holocene aridity. Quaternary Science Reviews 97, 84–101. https://doi.org/10.1016/j.quascirev.2014.05.005

Garcin, Y., Junginger, A., Melnick, D., Olago, D.O., Strecker, M.R., Trauth, M.H., 2009. Late Pleistocene–Holocene rise and collapse of Lake Suguta, northern Kenya Rift. Quaternary Science Reviews 28, 911–925. https://doi.org/10.1016/j.quascirev.2008.12.006

Garcin, Y., Melnick, D., Strecker, M.R., Olago, D., Tiercelin, J.-J., 2012. East African mid-Holocene wet–dry transition recorded in palaeo-shorelines of Lake Turkana, northern Kenya Rift. Earth and Planetary Science Letters 331–332, 322–334. https://doi.org/10.1016/j.epsl.2012.03.016

Garcin, Y., Vincens, A., Williamson, D., Buchet, G., Guiot, J., 2007. Abrupt resumption of the African Monsoon at the Younger Dryas—Holocene climatic transition. Quaternary Science Reviews 26, 690–704. https://doi.org/10.1016/j.quascirev.2006.10.014

Gasse, F., 2000. Hydrological changes in the African tropics since the Last Glacial Maximum. Quaternary Science Reviews 19, 189–211.

Gasse, F., 1990. Tectonic and Climatic Controls on Lake Distribution and Environments in Afar from Miocene to Present, in: Lacustrine BAsin Exploration - Cases Studies and Modern Analogs, AAPG Memoir. pp. 19–41.

Gasse, F., 1977. Evolution of Lake Abhe (T.F.A.I.), from 70,000 BP. Nature 265, 42–45.

Gasse, F., 1975. L'évolution des lacs de l'Afar Central (Ethiopie et T.F.A.I.) du Plio-Pléistocène à l'Actuel. Recostitution des paléomilieux lacustres à partir de l'étude des Diatomées. Université de Paris VI, Paris.

Gasse, F., Chalié, F., Vincens, A., Williams, M.A.J., Williamson, D., 2008. Climatic patterns in equatorial and southern Africa from 30,000 to 10,000 years ago reconstructed from terrestrial and near-shore proxy data. Quaternary Science Reviews 27, 2316–2340. https://doi.org/10.1016/j.quascirev.2008.08.027

Gasse, F., Rognon, P., Street, F.A., 1980. Quaternary history of the Afar and Ethiopian Rift lakes., in: The Sahare an the Nile. Quaternary Environments and Prehistoric Occupation in Northern Africa. Williams A.J. Martin, Faurue Huges, pp. 361–400.

Gasse, F., Street, F.A., 1978. Late Quaternary lake-level fluctuations and environments of the northern Rift Valley and Afar region (Ethiopia and Djibouti). Palaeogeography, Palaeoclimatology, Palaeoecology 24, 279297299–295325.

Ghinassi, M., D'Oriano, F., Benvenuti, M., Awramik, S., Bartolini, C., Fedi, M., Ferrari, G., Papini, M., Sagri, M., Talbot, M., 2012. Shoreline fluctuations of Lake Hayk (northern Ethiopia) during the last 3500years: Geomorphological, sedimentary, and isotope records. Palaeogeography, Palaeoclimatology, Palaeoecology 365–366, 209–226. https://doi.org/10.1016/j.palaeo.2012.09.029

Gilbert, G.K., 1885. Topographic Features of Lake Shores. US Geol. Surv. Ann. Rep. 5, 69–123.

Gillespie, R., Street-Perrot, A., Switsur, R., 1983. Post-glacial arid episodes in Ethiopia have implications for climate prediction. Nature 306, 680–683.

Gobo, K., Ghinassi, M., Nemec, W., 2015. Gilbert-type deltas recording short-term base-level changes: Delta-brink morphodynamics and related foreset facies. Sedimentology 62, 1923–1949. https://doi.org/10.1111/sed.12212

Gobo, K., Ghinassi, M., Nemec, W., 2014. Reciprocal Changes In Foreset To Bottomset Facies In A Gilbert-Type Delta: Response To Short-Term Changes In Base Level. Journal of Sedimentary Research 84, 1079–1095. https://doi.org/10.2110/jsr.2014.83

Grandin, R., Jacques, E., Nercessian, A., Ayele, A., Doubre, C., Socquet, A., Keir, D., Kassim, M., Lemarchand, A., King, G.C.P., 2011. Seismicity during lateral dike propagation: Insights from new data in the recent Manda Hararo-Dabbahu rifting episode (Afar, Ethiopia): DIKE-INDUCED SEISMICITY IN AFAR. Geochem. Geophys. Geosyst. 12, n/a-n/a. https://doi.org/10.1029/2010GC003434

Grandin, R., Socquet, A., Binet, R., Klinger, Y., Jacques, E., de Chabalier, J.-B., King, G.C.P., Lasserre, C., Tait, S., Tapponnier, P., Delorme, A., Pinzuti, P., 2009. September 2005 Manda Hararo-Dabbahu rifting event, Afar (Ethiopia): Constraints provided by geodetic data. J. Geophys. Res. 114, B08404. https://doi.org/10.1029/2008JB005843

Grove, A.T., Goudie, A.S., 1971. Late Quaternary Lake Levels in the Rift Valley of Southern Ethiopia and Elsewhere in Tropical Africa. Nature 234, 403–405. https://doi.org/10.1038/234403a0

Hailemichael, M., Aronson, J.L., Savin, S., Tevesz, M.J.S., Carter, J.G., 2002. δ18O in mollusk shells from Pliocene Lake Hadar and modern Ethiopian lakes: implications for history of the Ethiopian monsoon. Palaeogeography, Palaeoclimatology, Palaeoecology 186, 81–99. https://doi.org/10.1016/S0031-0182(02)00445-5

Harris, I., Jones, P.D., Osborn, T.J., Lister, D.H., 2014. Updated high-resolution grids of monthly climatic observations - the CRU TS3.10 Dataset: UPDATED HIGH-RESOLUTION GRIDS OF MONTHLY CLIMATIC OBSERVATIONS. Int. J. Climatol. 34, 623–642. https://doi.org/10.1002/joc.3711

Haug, G.H., 2001. Southward Migration of the Intertropical Convergence Zone Through the Holocene. Science 293, 1304–1308. https://doi.org/10.1126/science.1059725

Hesp, P.A., 2006. Sand Beach Ridges: Definitions and Re-Definition. Journal of Coastal Research 72–75.

Hillaire-Marcel, C., Carro, O., Casanova, J., 1986. 14 C and Th/U dating of Pleistocene and Holocene stromatolites from East African paleolakes. Quaternary Research 25, 312–239.

Hofmann, C., Courtillot, V., Féraud, G., Rochette, P., Yirgu, G., Ketefo, E., Pik, R., 1997. Timing of the Ethiopian flood basalt event and implications for plume birth and global change. Nature 389, 838–841. https://doi.org/10.1038/39853

Holmes, J., Hoelzmann, P., 2017. The Late Pleistocene-Holocene African Humid Period as Evident in Lakes. Oxford University Press. https://doi.org/10.1093/acrefore/9780190228620.013.531

Hopcroft, P.O., Valdes, P.J., Harper, A.B., Beerling, D.J., 2017. Multi vegetation model evaluation of the Green Sahara climate regime: RAINFALL SUPPORTING A GREEN SAHARA. Geophysical Research Letters 44, 6804–6813. https://doi.org/10.1002/2017GL073740

Junginger, A., Roller, S., Olaka, L.A., Trauth, M.H., 2014. The effects of solar irradiation changes on the migration of the Congo Air Boundary and water levels of paleo-Lake Suguta, Northern Kenya Rift, during the African Humid Period (15–5ka BP). Palaeogeography, Palaeoclimatology, Palaeoecology 396, 1–16. https://doi.org/10.1016/j.palaeo.2013.12.007

Junginger, A., Trauth, M.H., 2013. Hydrological constraints of paleo-Lake Suguta in the Northern Kenya Rift during the African Humid Period (15–5kaBP). Global and Planetary Change 111, 174–188. https://doi.org/10.1016/j.gloplacha.2013.09.005

Khalidi, L., Mologni, C., Ménard, C., Coudert, L., Gabriele, M., Davtian, G., Cauliez, J., Lesur, J., Bruxelles, L., Chesnaux, L., Redae, B.E., Hainsworth, E., Doubre, C., Revel, M., Schuster, M., Zazzo, A., 2020. 9000 years of human lakeside adaptation in the Ethiopian Afar: Fisher-foragers and the first pastoralists in the Lake Abhe basin during the African Humid Period. Quaternary Science Reviews 243, 106459. https://doi.org/10.1016/j.quascirev.2020.106459

Kidane, T., Courtillot, V., Manighetti, I., Audin, L., Lahitte, P., Quidelleur, X., Gillot, P.-Y., Gallet, Y., Carlut, J., Haile, T., 2003. New paleomagnetic and geochronologic results from Ethiopian Afar: Block rotations linked to rift overlap and propagation and determination of a ~2 Ma reference pole for stable Africa: NEW PALEOMAGNETIC AND GEOCHRONOLOGIC RESULTS. J. Geophys. Res. 108. https://doi.org/10.1029/2001JB000645

Kutzbach, J.E., Street-Perrott, F.A., 1985. Milankovitch forcing of fluctuations in the level of tropical lakes from 18 to 0 kyr BP. Nature 317, 130–134. https://doi.org/10.1038/317130a0

Lamb, H.F., Bates, C.R., Bryant, C.L., Davies, S.J., Huws, D.G., Marshall, M.H., Roberts, H.M., 2018. 150,000-year palaeoclimate record from northern Ethiopia supports early, multiple dispersals of modern humans from Africa. Scientific Reports 8. https://doi.org/10.1038/s41598-018-19601-w

Macgregor, D., 2015. History of the development of the East African Rift System: A series of interpreted maps through time. Journal of African Earth Sciences 101, 232–252. https://doi.org/10.1016/j.jafrearsci.2014.09.016

Manighetti, I., Tapponnier, P., Courtillot, V., Gallet, Y., Jacques, E., Gillot, P.-Y., 2001. Strain transfer between disconnected, propagating rifts in Afar. J. Geophys. Res. 106, 13613–13665. https://doi.org/10.1029/2000JB900454

Manighetti, I., Tapponnier, P., Gillot, P.Y., Jacques, E., Courtillot, V., Armijo, R., Ruegg, J.C., King, G., 1998. Propagation of rifting along the Arabia-Somalia Plate Boundary: Into Afar. J. Geophys. Res. 103, 4947–4974. https://doi.org/10.1029/97JB02758

Marzin, C., Braconnot, P., 2009. The role of the ocean feedback on Asian and African monsoon variations at 6kyr and 9.5kyr BP. Comptes Rendus Geoscience 341, 643–655. https://doi.org/10.1016/j.crte.2009.09.001

Massari, F., Colella, A., 1988. Evolution and types of fan–delta systems in some major tectonic settings, in: Fan Deltas: Sedimentology and Tectonic Settings. Blackie, London, pp. 103–122.

Melnick, D., Garcin, Y., Quinteros, J., Strecker, M.R., Olago, D., Tiercelin, J.-J., 2012. Steady rifting in northern Kenya inferred from deformed Holocene lake shorelines of the Suguta and Turkana basins. Earth and Planetary Science Letters 331–332, 335–346. https://doi.org/10.1016/j.epsl.2012.03.007

Ménot, G., Pivot, S., Bouloubassi, I., Davtian, N., Hennekam, R., Bosch, D., Ducassou, E., Bard, E., Migeon, S., Revel, M., 2020. Timing and stepwise transitions of the African Humid Period from geochemical proxies in the Nile deep-sea fan sediments. Quaternary Science Reviews 228, 106071. https://doi.org/10.1016/j.quascirev.2019.106071

Mohtadi, M., Prange, M., Steinke, S., 2016. Palaeoclimatic insights into forcing and response of monsoon rainfall. Nature 533, 191–199. https://doi.org/10.1038/nature17450

Mologni, C., Revel, M., Blanchet, C., Bosch, D., Develle, A.-L., Orange, F., Bastian, L., Khalidi, L., Ducassou, E., Migeon, S., 2020. Frequency of exceptional Nile flood events as an indicator of Holocene hydro-climatic changes in the Ethiopian Highlands. Quaternary Science Reviews 247, 106543. https://doi.org/10.1016/j.quascirev.2020.106543

Nilsson, E., 1940. Ancient Changes of Climate in British East Africa and Abyssinia. A Study of Ancient Lakes and Glaciers. Geografiska Annaler 22, 1. https://doi.org/10.2307/519977

Overpeck, J., Anderson, D., Trumbore, S., Prell, W., 1996. The southwest Indian Monsoon over the last 18 000 years. Climate Dynamics 12, 213–225. https://doi.org/10.1007/BF00211619

Pagli, C., Wang, H., Wright, T.J., Calais, E., Lewi, E., 2014. Current plate boundary deformation of the Afar rift from a 3-D velocity field inversion of InSAR and GPS: Current Afar plate boundary deformation. J. Geophys. Res. Solid Earth 119, 8562–8575. https://doi.org/10.1002/2014JB011391

Rasmussen, S.O., Bigler, M., Blockley, S.P., Blunier, T., Buchardt, S.L., Clausen, H.B., Cvijanovic, I., Dahl-Jensen, D., Johnsen, S.J., Fischer, H., Gkinis, V., Guillevic, M., Hoek, W.Z., Lowe, J.J., Pedro, J.B., Popp, T., Seierstad, I.K., Steffensen, J.P., Svensson, A.M., Vallelonga, P., Vinther, B.M., Walker, M.J.C., Wheatley, J.J., Winstrup, M., 2014. A stratigraphic framework for abrupt climatic changes during the Last Glacial period based on three synchronized Greenland ice-core records: refining and extending the INTIMATE event stratigraphy. Quaternary Science Reviews 106, 14–28. https://doi.org/10.1016/j.quascirev.2014.09.007

Reimer, P.J., Bard, E., Bayliss, A., Beck, J.W., Blackwell, P.G., Ramsey, C.B., Buck, C.E., Cheng, H., Edwards, R.L., Friedrich, M., Grootes, P.M., Guilderson, T.P., Haflidason, H., Hajdas, I., Hatté, C., Heaton, T.J., Hoffmann, D.L., Hogg, A.G., Hughen, K.A., Kaiser, K.F., Kromer, B., Manning, S.W., Niu, M., Reimer, R.W., Richards, D.A., Scott, E.M., Southon, J.R., Staff, R.A., Turney, C.S.M., van der Plicht, J., 2013. IntCal13 and Marine13 Radiocarbon Age Calibration Curves 0–50,000 Years cal BP. Radiocarbon 55, 1869–1887. https://doi.org/10.2458/azu_js_rc.55.16947

Revel, M., Ducassou, E., Skonieczny, C., Colin, C., Bastian, L., Bosch, D., Migeon, S., Mascle, J., 2015. 20,000 years of Nile River dynamics and environmental changes in the Nile catchment area as inferred from Nile upper continental slope sediments. Quaternary Science Reviews 130, 200–221. https://doi.org/10.1016/j.quascirev.2015.10.030

Richardson, J.L., Dussinger, R.A., 1986. Paleolimnology of mid-elevation lakes in the Kenya Rift Valley. Hydrobiologia 143, 167–174.

Rognon, P., Gasse, F., 1973. Depots lacustres quaternaires de la basse vallée de l’Awash (Afar, Ethiopie): leurs rapports avec la techtonique et le volcanisme sous-aquatique. Révue de Gèographie Physique et de Géologie Dynamique XV, 295–316.

Rohling, E.J., Pälike, H., 2005. Centennial-scale climate cooling with a sudden cold event around 8,200 years ago. Nature 434, 975–979. https://doi.org/10.1038/nature03421

Rossignol-Strick, M., Nesteroff, W., Olive, P., Vergnaud-Grazzini, C., 1982. After the deluge: Mediterranean stagnation and sapropel formation. Nature 295, 105–110. https://doi.org/10.1038/295105a0

Sagri, M., Bartolini, C., Billi, P., Ferrari, G., Benvenuti, M., Carnicelli, S., Barbano, F., 2008. Latest Pleistocene and Holocene river network evolution in the Ethiopian Lakes Region. Geomorphology 94, 79–97. https://doi.org/10.1016/j.geomorph.2007.05.010

Schefuß, E., Eglinton, T.I., Spencer-Jones, C.L., Rullkötter, J., De Pol-Holz, R., Talbot, H.M., Grootes, P.M., Schneider, R.R., 2016. Hydrologic control of carbon cycling and aged carbon discharge in the Congo River basin. Nature Geosci 9, 687–690. https://doi.org/10.1038/ngeo2778

Schuster, M., Duringer, P., Ghienne, J.-F., Vignaud, P., Beauvilain, A., Mackaye, H.T., Brunet, M., 2003. Coastal conglomerates around the Hadjer el Khamis inselbergs (western Chad, central Africa): new evidence for Lake Mega-Chad episodes. Earth Surf. Process. Landforms 28, 1059–1069. https://doi.org/10.1002/esp.502

Schuster, M., Nutz, A., 2018. Lacustrine wave-dominated clastic shorelines: modern to ancient littoral landforms and deposits from the Lake Turkana Basin (East African Rift System, Kenya). J Paleolimnol 59, 221–243. https://doi.org/10.1007/s10933-017-9960-4

Shanahan, T.M., McKay, N.P., Hughen, K.A., Overpeck, J.T., Otto-Bliesner, B., Heil, C.W., King, J., Scholz, C.A., Peck, J., 2015. The time-transgressive termination of the African Humid Period. Nature Geoscience 8, 140–144. https://doi.org/10.1038/ngeo2329

Skonieczny, C., McGee, D., Winckler, G., Bory, A., Bradtmiller, L.I., Kinsley, C.W., Polissar, P.J., De Pol-Holz, R., Rossignol, L., Malaizé, B., 2019. Monsoon-driven Saharan dust variability over the past 240,000 years. Sci. Adv. 5, eaav1887. https://doi.org/10.1126/sciadv.aav1887

Smith, D.G., Jol, H.M., 1997. Radar structure of a Gilbert-type delta, Peyto Lake, Banff National Park, Canada. Sedimentary Geology 113, 195–209. https://doi.org/10.1016/S0037-0738(97)00061-4

Stamps, D.S., Flesch, L.M., Calais, E., Ghosh, A., 2014. Current kinematics and dynamics of Africa and the East African Rift System. J. Geophys. Res. Solid Earth 119, 5161–5186. https://doi.org/10.1002/2013JB010717

Stamps, D.S., Kreemer, C., Fernandes, R., Rajaonarison, T.A., Rambolamanana, G., 2020. Redefining East African Rift System kinematics. Geology. https://doi.org/10.1130/G47985.1

Stein, R.S., Briole, P., Ruegg, J.-C., Tapponnier, P., Gasse, F., 1991. Contemporary, Holocene, and Quaternary deformation of the Asal Rift, Djibouti: Implications for the mechanics of slow spreading ridges. J. Geophys. Res. 96, 21789–21806. https://doi.org/10.1029/91JB02118

Sunamura, T., 1992. Geomorphology of Rocky Coasts, Wiley. ed.

Tapponnier, P., Armijo, R., Manighetti, I., Courtillot, V., 1990. Bookshelf faulting and horizontal block rotations between overlapping rifts in southern Afar. Geophys. Res. Lett. 17, 1–4. https://doi.org/10.1029/GL017i001p00001

Temtime, T., Biggs, J., Lewi, E., Hamling, I., Wright, T., Ayele, A., 2018. Spatial and temporal patterns of deformation at the Tendaho geothermal prospect, Ethiopia. Journal of Volcanology and Geothermal Research 357, 56–67. https://doi.org/10.1016/j.jvolgeores.2018.04.004

Tiercelin, J.-J., 1981. Rifts contintntaux. Tectonique, climats, sédiments. Exemples: la sédimentation dans le nord du Rift Gregory (Kenya) et dans le Rift de l’Afar (Ethiopie) depuis le Miocéne (Thèse Doct. Etat). Univ. Aix-Marseille II.

Tiercelin, J.-J., Lezzar, K.-E., 2002. A 300 Million Years History of Rift Lakes in Central and East Africa: An Updated Broad Review, in: Odada, E.O., Olago, D.O. (Eds.), The East African Great Lakes: Limnology, Palaeolimnology and Biodiversity, Advances in Global Change Research. Springer Netherlands, Dordrecht, pp. 3–60. https://doi.org/10.1007/0-306-48201-0_1

Tierney, J.E., Russell, J.M., Sinninghe Damsté, J.S., Huang, Y., Verschuren, D., 2011. Late Quaternary behavior of the East African monsoon and the importance of the Congo Air Boundary. Quaternary Science Reviews 30, 798–807. https://doi.org/10.1016/j.quascirev.2011.01.017

Trauth, M.H., Maslin, M.A., Deino, A.L., Junginger, A., Lesoloyia, M., Odada, E.O., Olago, D.O., Olaka, L.A., Strecker, M.R., Tiedemann, R., 2010. Human evolution in a variable environment: the amplifier lakes of Eastern Africa. Quaternary Science Reviews 29, 2981–2988. https://doi.org/10.1016/j.quascirev.2010.07.007

Trenhaile, A.S., 2015. Coastal notches: Their morphology, formation, and function. Earth-Science Reviews 150, 285–304. https://doi.org/10.1016/j.earscirev.2015.08.003

Tuenter, E., Weber, S.L., Hilgen, F.J., Lourens, L.J., 2003. The response of the African summer monsoon to remote and local forcing due to precession and obliquity. Global and Planetary Change 36, 219–235. https://doi.org/10.1016/S0921-8181(02)00196-0

Varet, J., 2018. Geology of Afar (East Africa), Springer. ed, Regional Geology Reviews.

Viste, E., Sorteberg, A., 2013. Moisture transport into the Ethiopian highlands: MOISTURE TRANSPORT INTO THE ETHIOPIAN HIGHLANDS. Int. J. Climatol. 33, 249–263. https://doi.org/10.1002/joc.3409

Wood, R.B., Telling, J.F., 1988. Chemical and algal relationships in a salinity series of Ethiopian inland waters. Hydrobiologia 158, 29–67.

Fig 1

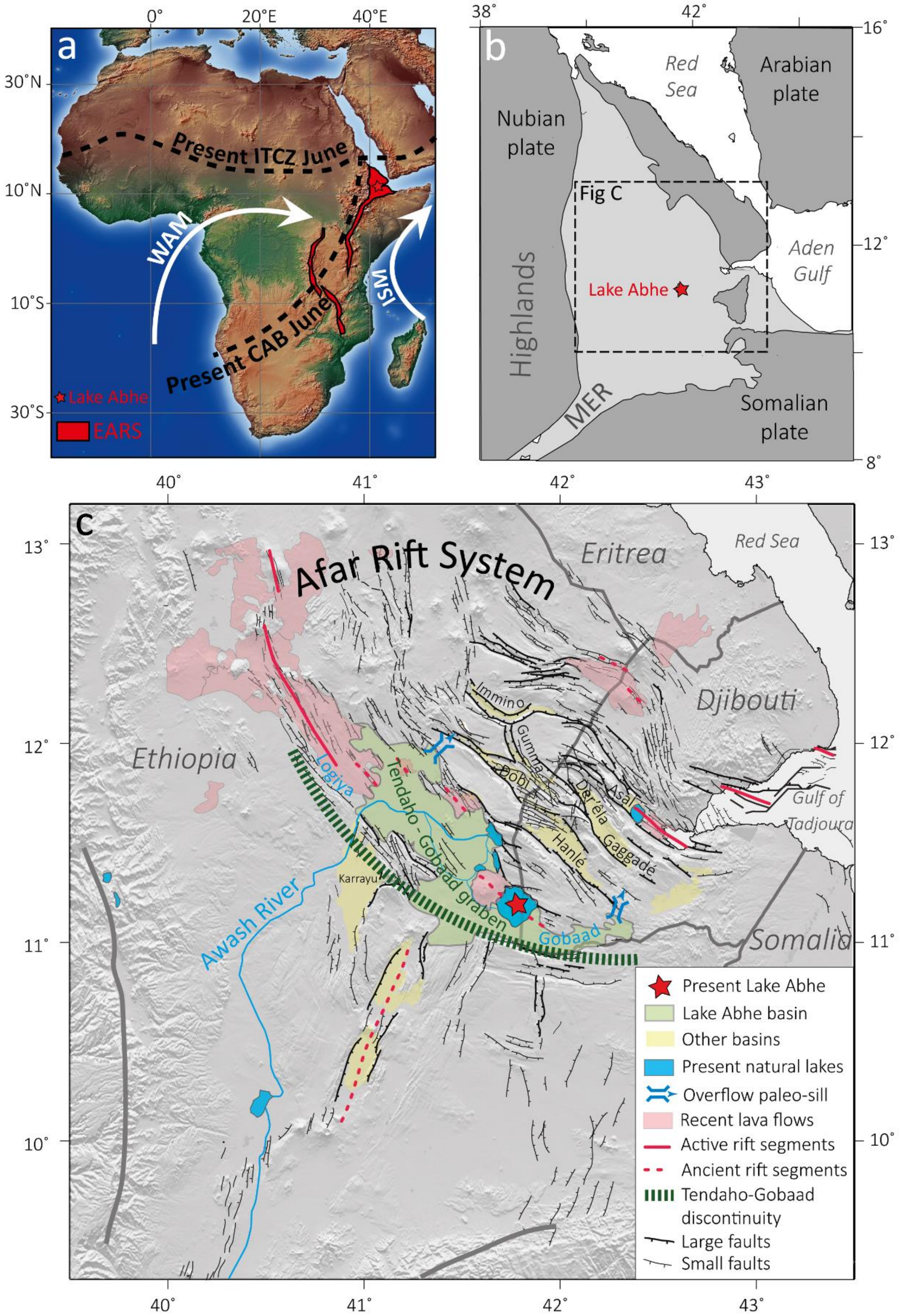
a
0°
20°E
40°E
30°N
10°N
10°S
30°S
Present ITCZ June
WAM
ISM
Present CAB June
Lake Abhe
EARS
b
38°
42°
16°
12°
8°
Red Sea
Arabian plate
Nubian plate
Fig C
Aden Gulf
Highlands
Lake Abhe
MER
Somalian plate
c
40°
41°
42°
43°
13°
12°
11°
10°
Afar Rift System
Eritrea
Red Sea
Djibouti
Ethiopia
Immino
Gumma
Dobi
Der'éla
Asal
Hanlé
Gaggade
Gulf of Tadjoura
Logiya
Tendaho - Gobaad graben
Karrayu
Awash River
Gobaad
Somalia
Present Lake Abhe
Lake Abhe basin
Other basins
Present natural lakes
Overflow paleo-sill
Recent lava flows
Active rift segments
Ancient rift segments
Tendaho-Gobaad discontinuity
Large faults
Small faults

Fig 2

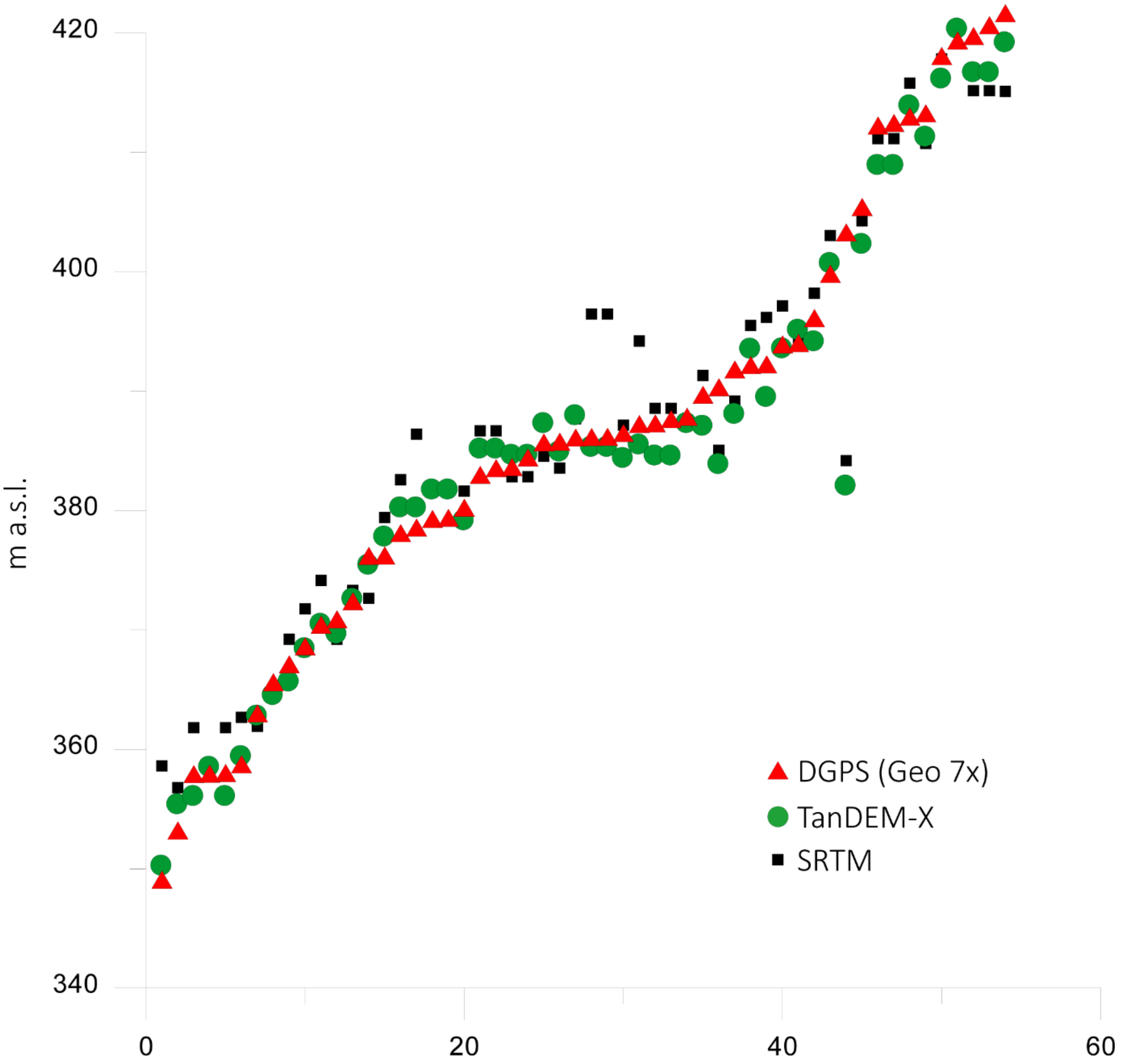

Fig 3


a
Wave abrasion notches
Beach pebbles/cobbles
b
paleo-shoreline
Abrasion platform
c
Abrasion platform on bedrock
Abrasion platform on sediments
d
Feeder canyon
Apex delta
Abrasion platform
e
Foreset
Bottomset
Lacustrine

Fig 4

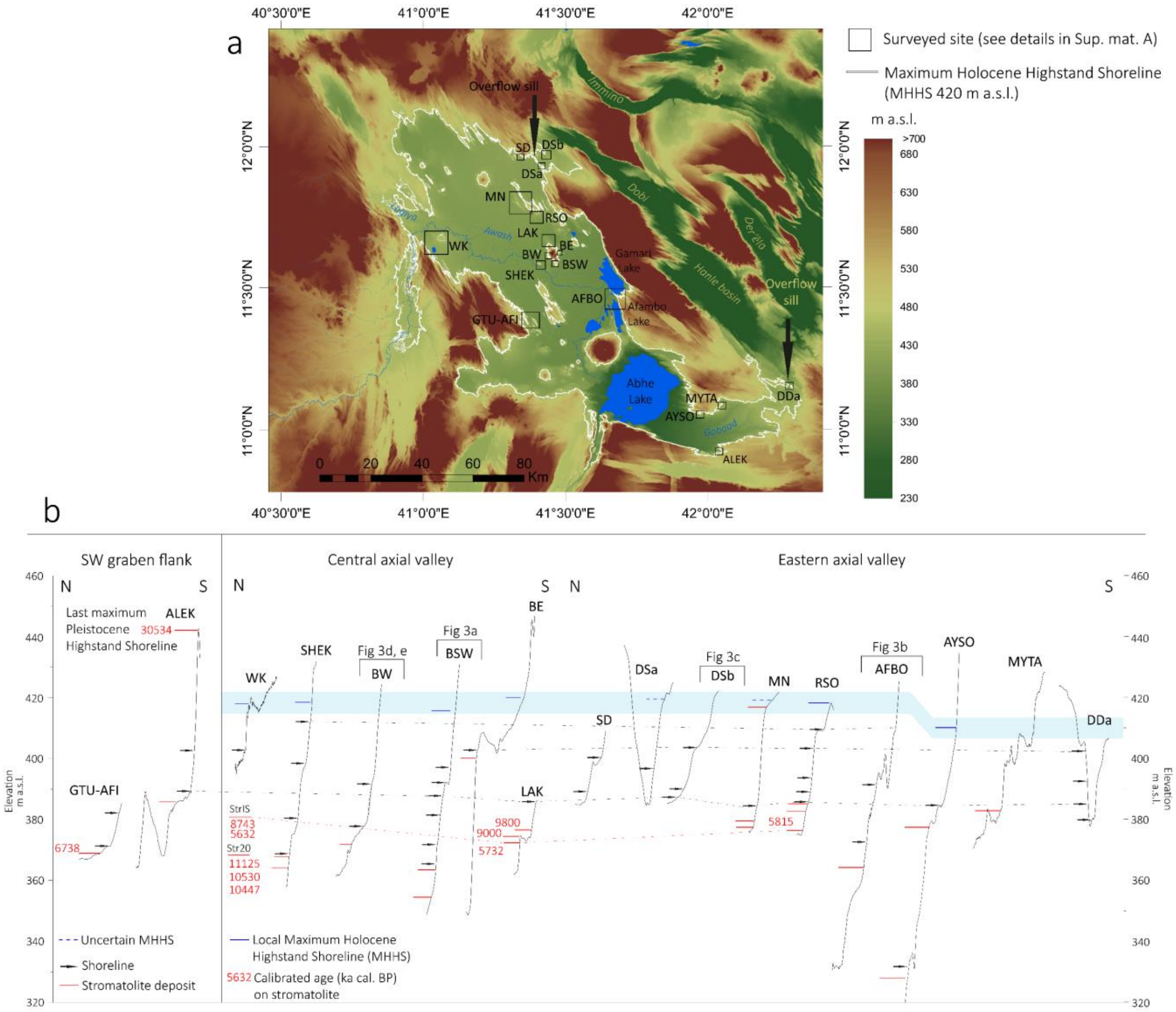
a
40°30'0"E
41°0'0"E
41°30'0"E
42°0'0"E
12°0'0"N
11°30'0"N
11°0'0"N
Surveyed site (see details in Sup. mat. A)
Maximum Holocene Highstand Shoreline (MHHS 420 m a.s.l.)
m a.s.l.
>700
680
630
580
530
480
430
380
330
280
230
Overflow sill
SD
DSb
DSa
MN
RSO
LAK
BE
BW
BSW
SHEK
WK
GTU-AFI
AFBO
Gamari Lake
Afambo Lake
Abhe Lake
MYTA
AYSO
DDa
ALEK
Immino
Dobi
Der'ela
Hanle basin
Awash
Gobaad
Overflow sill
0 20 40 60 80 Km
b
SW graben flank
Central axial valley
Eastern axial valley
N
S
Elevation m a.s.l.
460
440
420
400
380
360
340
320
Last maximum Pleistocene Highstand Shoreline
ALEK
30534
GTU-AFI
6738
WK
SHEK
Fig 3d, e
BW
Fig 3a
BSW
BE
LAK
SD
DSa
Fig 3c
DSb
MN
RSO
Fig 3b
AFBO
AYSO
MYTA
DDa
StrIS
8743
5632
Str20
11125
10530
10447
9800
9000
5732
5815
Uncertain MHHS
Shoreline
Stromatolite deposit
Local Maximum Holocene Highstand Shoreline (MHHS)
5632 Calibrated age (ka cal. BP) on stromatolite

Fig 5

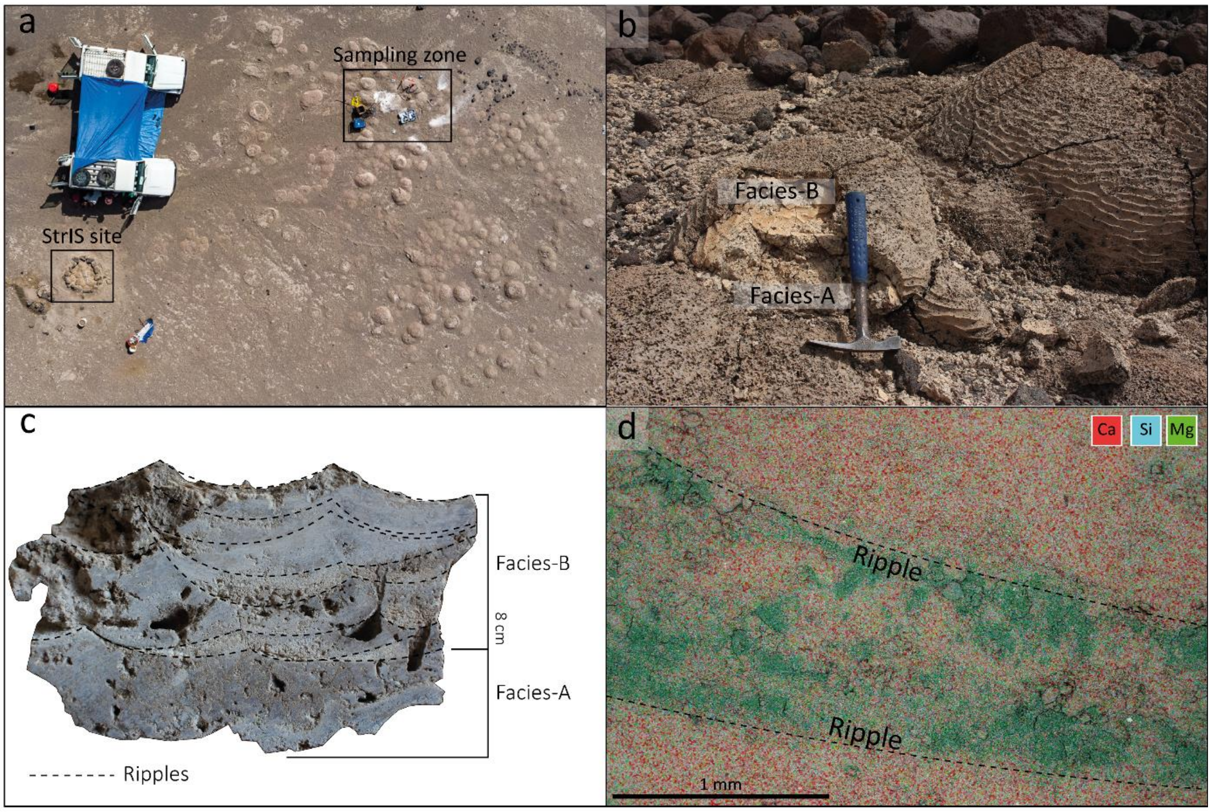
a
Sampling zone
StrIS site
b
Facies-B
Facies-A
c
Facies-B
8 cm
Facies-A
Ripples
d
Ca
Si
Mg
Ripple
Ripple
1 mm

Fig 6

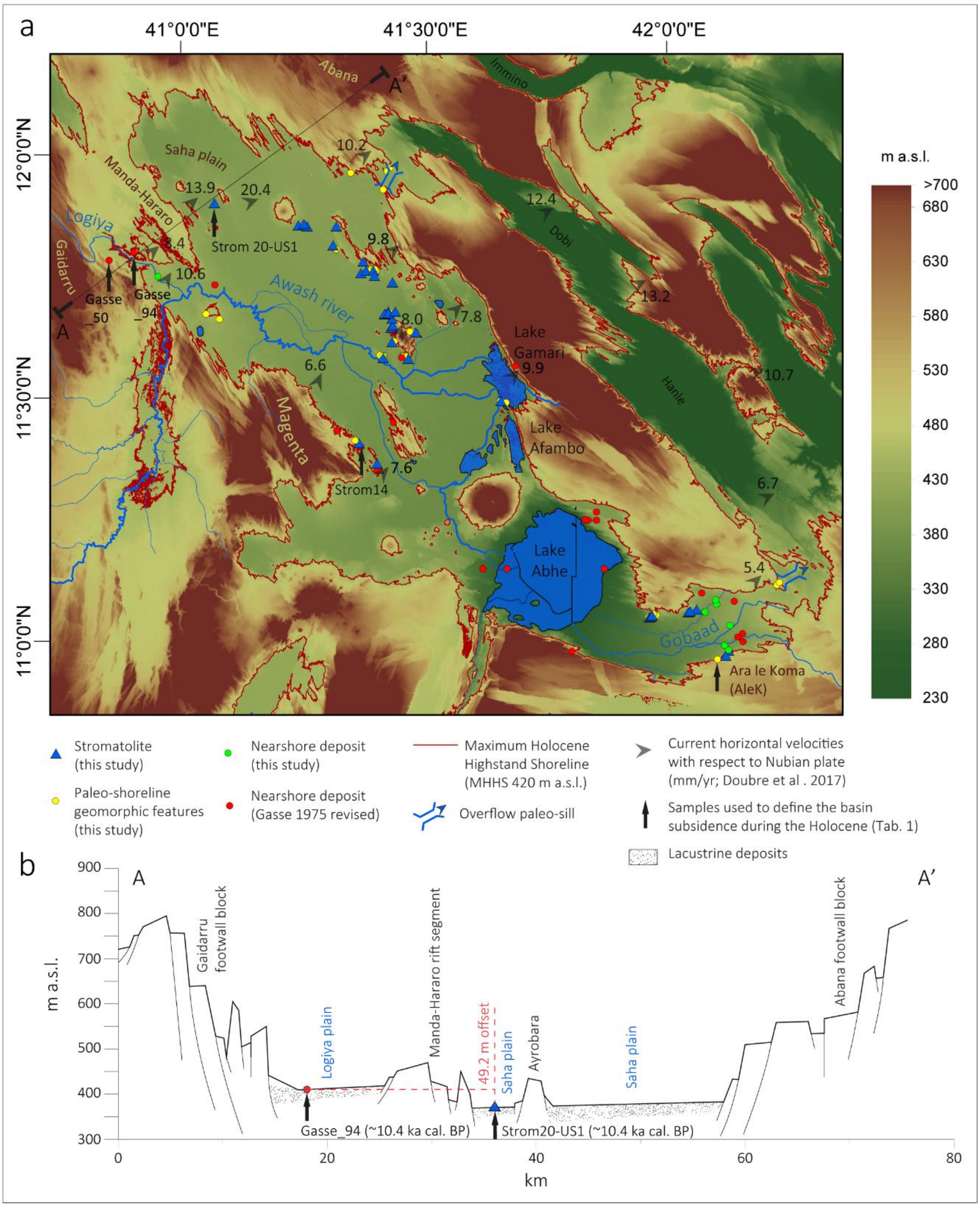
a
41°0'0"E
41°30'0"E
42°0'0"E
12°0'0"N
11°30'0"N
11°0'0"N
Abana
A'
Immino
Saha plain
Manda-Hararo
Logiya
Gaidarru
10.2
13.9
20.4
Strom 20-US1
12.4
Dobi
9.8
8.4
10.6
Gasse _50
Gasse _94
Awash river
A
8.0
7.8
13.2
Lake Gamari
9.9
6.6
10.7
Hanle
Magenta
Lake Afambo
Strom14
7.6
6.7
Lake Abhe
5.4
Gobaad
Ara le Koma (AleK)
m a.s.l.
>700
680
630
580
530
480
430
380
330
280
230
Stromatolite (this study)
Paleo-shoreline geomorphic features (this study)
Nearshore deposit (this study)
Nearshore deposit (Gasse 1975 revised)
Maximum Holocene Highstand Shoreline (MHHS 420 m a.s.l.)
Overflow paleo-sill
Current horizontal velocities with respect to Nubian plate (mm/yr; Doubre et al . 2017)
Samples used to define the basin subsidence during the Holocene (Tab. 1)
Lacustrine deposits
b
900
800
700
600
500
400
300
m a.s.l.
A
A'
Gaidarru footwall block
Logiya plain
Manda-Hararo rift segment
49.2 m offset
Saha plain
Ayrobara
Saha plain
Abana footwall block
Gasse_94 (~10.4 ka cal. BP)
Strom20-US1 (~10.4 ka cal. BP)
0
20
40
60
80
km

Fig 7

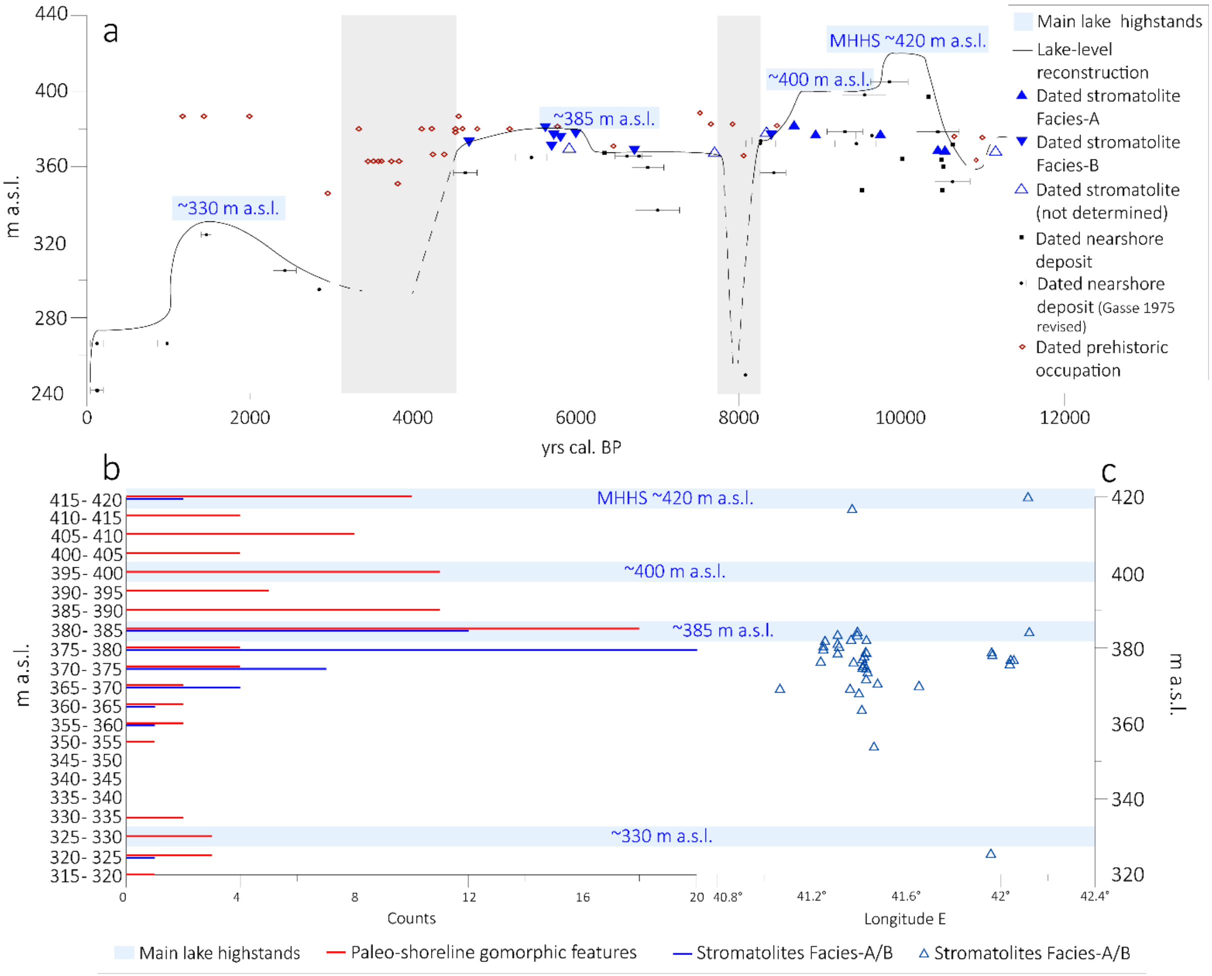
a
440
400
360
320
280
240
m a.s.l.
0
2000
4000
6000
8000
10000
12000
yrs cal. BP
~330 m a.s.l.
~385 m a.s.l.
~400 m a.s.l.
MHHS ~420 m a.s.l.
Main lake highstands
Lake-level reconstruction
Dated stromatolite Facies-A
Dated stromatolite Facies-B
Dated stromatolite (not determined)
Dated nearshore deposit
Dated nearshore deposit (Gasse 1975 revised)
Dated prehistoric occupation
b
415- 420
410- 415
405- 410
400- 405
395- 400
390- 395
385- 390
380- 385
375- 380
370- 375
365- 370
360- 365
355- 360
350- 355
345- 350
340- 345
335- 340
330- 335
325- 330
320- 325
315- 320
m a.s.l.
0
4
8
12
16
20
Counts
MHHS ~420 m a.s.l.
~400 m a.s.l.
~385 m a.s.l.
~330 m a.s.l.
c
420
400
380
360
340
320
m a.s.l.
40.8°
41.2°
41.6°
42°
42.4°
Longitude E
Main lake highstands
Paleo-shoreline gomorphic features
Stromatolites Facies-A/B
Stromatolites Facies-A/B

Fig 8

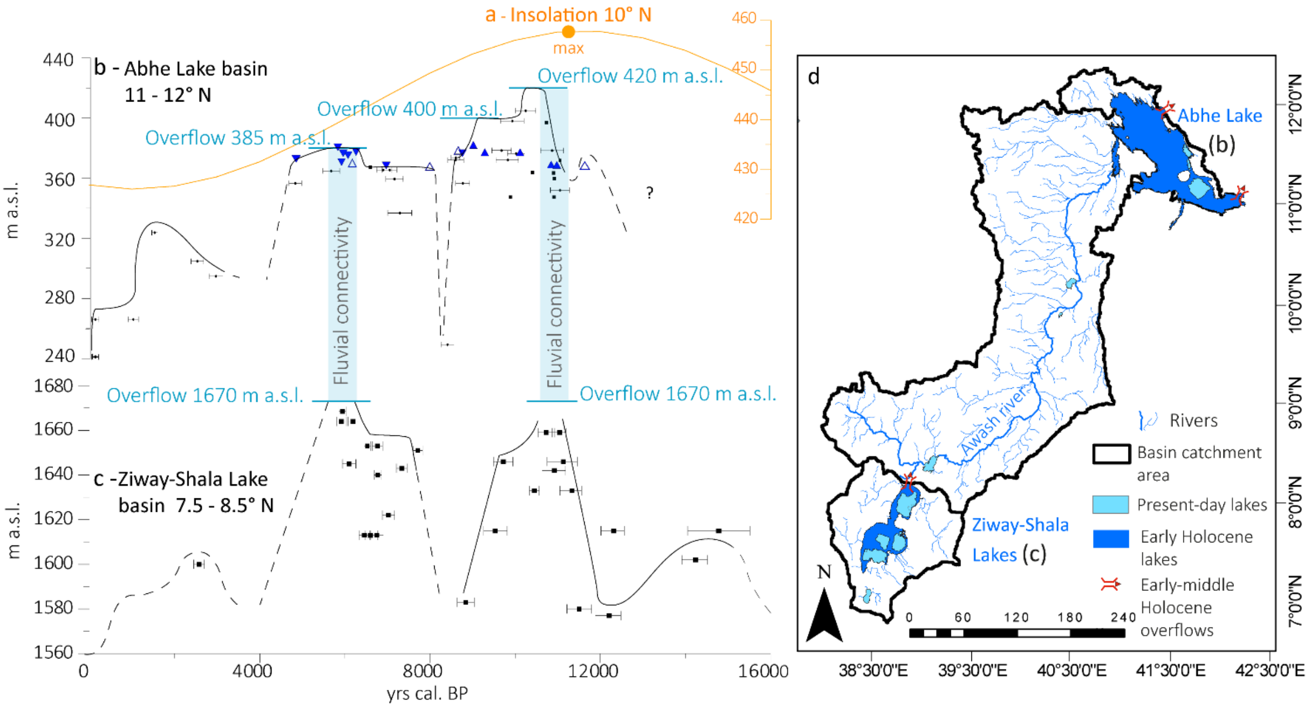
a - Insolation 10° N
max
460
450
440
430
420
b - Abhe Lake basin
11 - 12° N
Overflow 420 m a.s.l.
Overflow 400 m a.s.l.
Overflow 385 m a.s.l.
440
400
360
320
280
240
m a.s.l.
?
Fluvial connectivity
Fluvial connectivity
1680
Overflow 1670 m a.s.l.
Overflow 1670 m a.s.l.
1660
1640
c -Ziway-Shala Lake
basin 7.5 - 8.5° N
1620
1600
1580
1560
m a.s.l.
0
4000
8000
12000
16000
yrs cal. BP
d
Abhe Lake
(b)
Awash river
Ziway-Shala
Lakes (c)
Rivers
Basin catchment area
Present-day lakes
Early Holocene lakes
Early-middle Holocene overflows
N
0
60
120
180
240
12°0'0"N
11°0'0"N
10°0'0"N
9°0'0"N
8°0'0"N
7°0'0"N
38°30'0"E
39°30'0"E
40°30'0"E
41°30'0"E
42°30'0"E

Fig 9

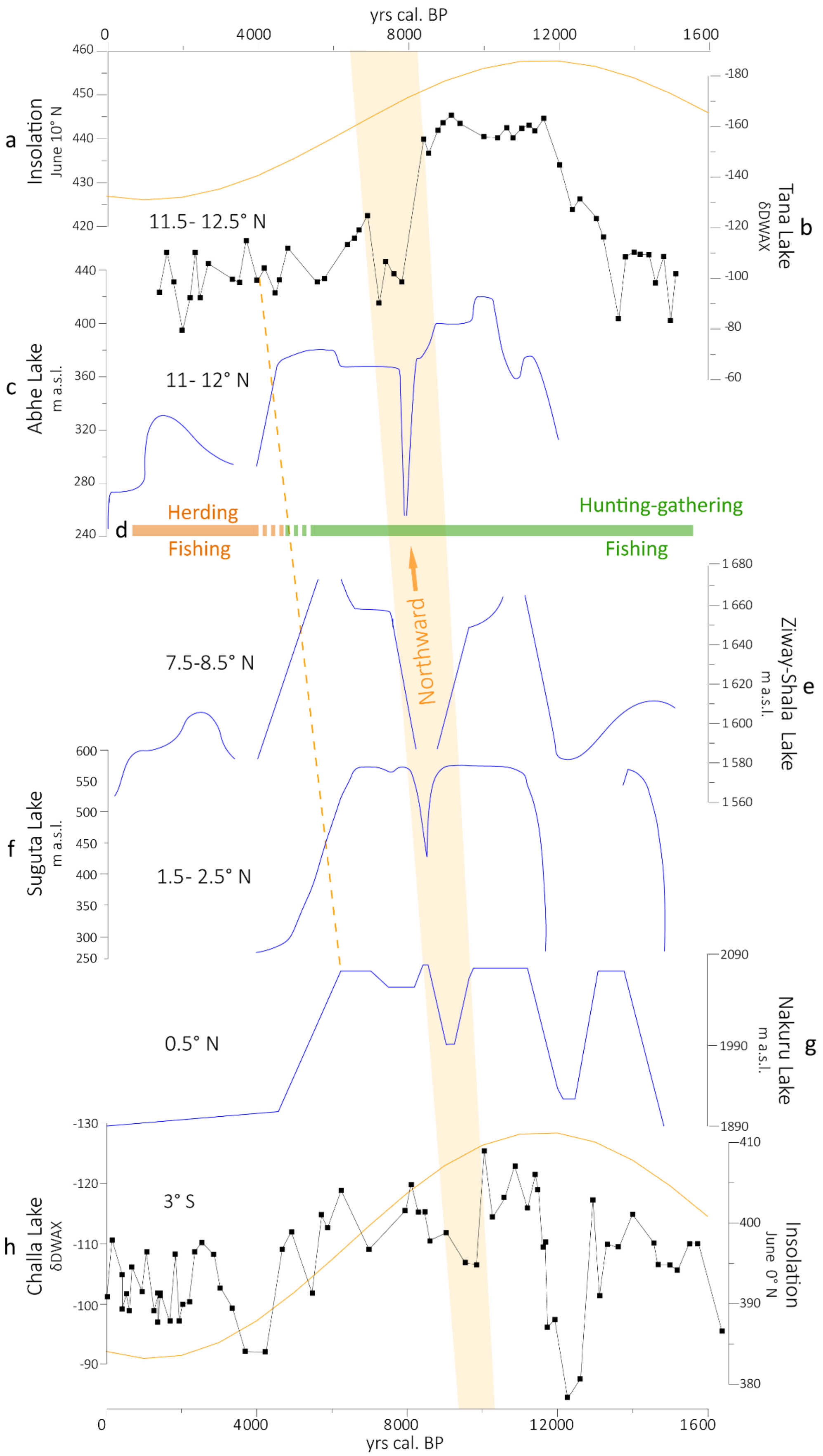
yrs cal. BP
0
4000
8000
12000
1600
a
Insolation
June 10° N
460
450
440
430
420
11.5- 12.5° N
-180
-160
-140
-120
-100
-80
-60
Tana Lake
δDWAX
b
c
Abhe Lake
m a.s.l.
440
400
360
320
280
240
11- 12° N
d
Herding
Fishing
Hunting-gathering
Fishing
Northward
7.5-8.5° N
1 680
1 660
1 640
1 620
1 600
1 580
1 560
Ziway-Shala Lake
m a.s.l.
e
f
Suguta Lake
m a.s.l.
600
550
500
450
400
350
300
250
1.5- 2.5° N
0.5° N
2090
1990
1890
Nakuru Lake
m a.s.l.
g
h
Challa Lake
δDWAX
-130
-120
-110
-100
-90
3° S
410
400
390
380
Insolation
June 0° N
0
4000
8000
12000
1600
yrs cal. BP

Fig 10

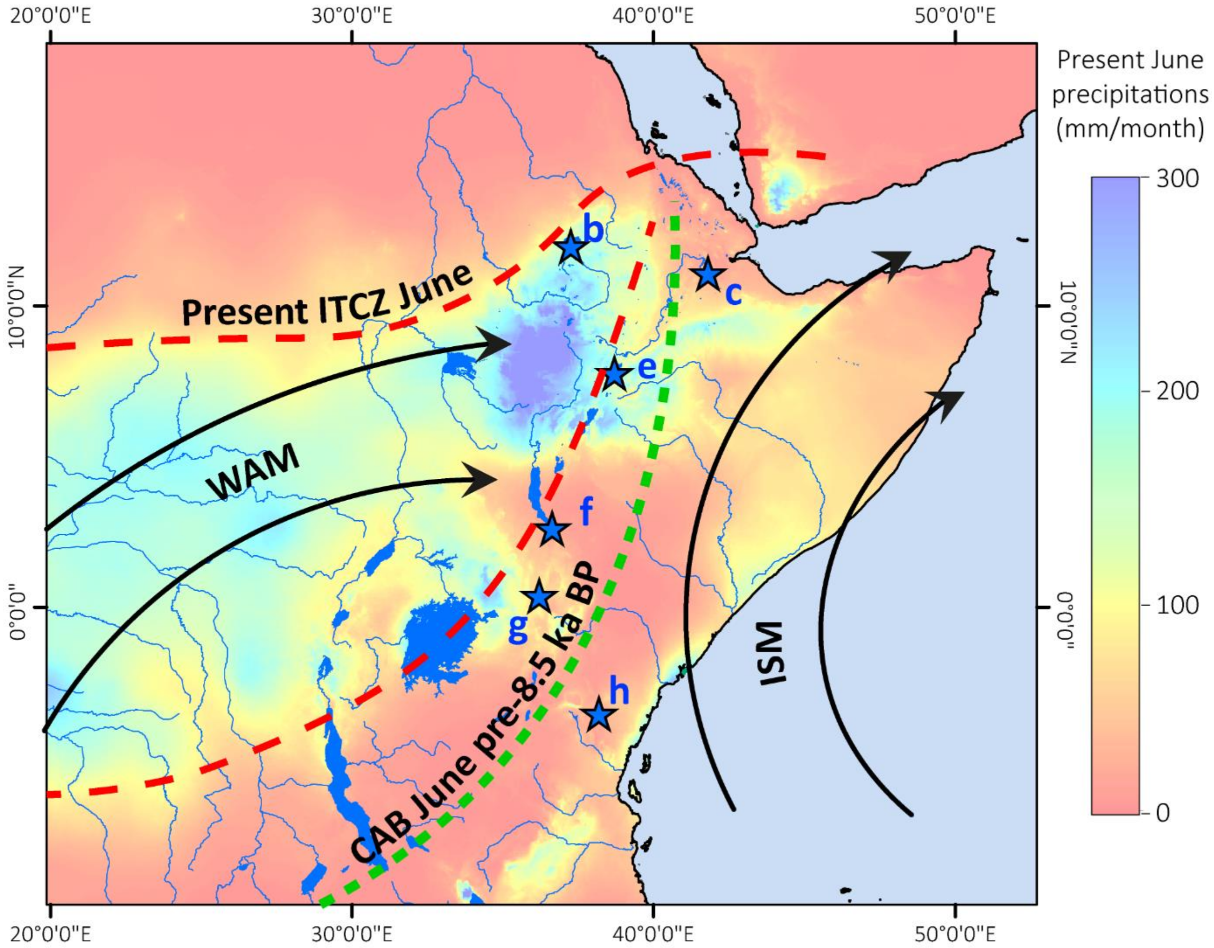
20°0'0"E
30°0'0"E
40°0'0"E
50°0'0"E
10°0'0"N
0°0'0"
Present June precipitations (mm/month)
300
200
100
0
Present ITCZ June
WAM
ISM
CAB June pre-8.5 ka BP
b
c
e
f
g
h

Table 1

ID	Lab ID	Age yr BP	Material	Cal ages yr BP (range 95.4 %)	Cal ages yr BP (median)	Elevations (TanDEMx +10m a.s.l.)	Subsidence rate (mm/yr)	Subsidence correction (m)	Corrected elevation (m a.s.l.)
Strom-ALEK-2	SacA62534	26250 ± 240	Str	30995-30082	30534 ± 248	440	/	/	/
Strom20-SU5	SacA58238	9689 ± 40	Str	11210-10805	11125 ± 113	369	/	/	/
Strom20-SU4	SacA58239	9320 ± 40	Str-A	10660-10404	10530 ± 64	369	/	/	/
Strom20-SU1	SacA58240	9265 ± 40	Str-A	10565-10295	10447 ± 73	369	/	/	/
Strom10a	SacA55608	8790 ± 30	Str-A	10112-9679	9807 ± 81	376.8	/	/	/
Strom10b	SacA55609	8075 ± 35	Str-A	9123-8785	9008 ± 70	376.8	/	/	/
Strom31	Poz-113925	7910 ± 50	Str-A	8978-8598	8743 ± 109	381.7	/	/	/
Strom49-bloc	Poz-124776	7620 ± 50	Str-B	8537-8350	8418 ± 46	377.6	/	/	/
Strom49-col	Poz-124778	7540 ± 50	Str	8419-8200	8360 ± 54	377.6	/	/	/
Strom14	Poz-124783	6870 ± 40	Str	7791-7614	7701 ± 44	367.7	/	/	/
Strom13	SacA55611	5919 ± 30	Str-B	6829-6666	6738 ± 40	369	/	/	/
Strom49-lam1a	Poz-124779	5255 ± 35	Str-B	6179-5929	6015 ± 73	377.6	/	/	/
Strom44	Poz-124781	5155 ± 35	Str	5995-5756	5918 ± 58	369.7	/	/	/
Raso2-Strom	Poz-113843	5085 ± 35	Str-B	5913-5746	5815 ± 51	376	/	/	/
Strom49-lam2a	Poz-124777	5015 ± 35	Str	5895-5608	5752 ± 71	377.6	/	/	/
Strom7	SacA55610	5005 ± 30	Str-B	5889-5653	5732 ± 69	371,5	/	/	/
Stromatolis-SU1	Poz-113841	4910 ± 30	Str-B	5712-5591	5632 ± 29	381.7	/	/	/

Strom51	Poz-124782	4160 ± 30	Str-B	4828-4580	4705 ± 69	373.3	/	/	/
2016-PSPCA-2	Poz-82850[‡]	9310 ± 50	*Mt (nearshore)*	10662-10298	10513 ± 82	360.3	/	/	/
2016-PSPCA-3	Poz-82851[‡]	9300 ± 50	*Mt (nearshore)*	10653-10296	10498 ± 83	348.1	/	/	/
2016-PSPCA-1	Poz-82849[‡]	8770 ± 50	*Mt (nearshore)*	10116-9552	9773 ± 126	364.5	/	/	/
2016-PSPCA-4	Poz-83625[‡]	5570 ± 35	*Mt (nearshore)*	6410-6294	6354 ± 33	367.6	/	/	/
2017-PSPCA-2	SacA55422[‡]	9290 ± 35	*Mt (nearshore)*	10583-10301	10491 ± 62	364	/	/	/
2017-PSPCA-3	SacA55425[‡]	9395 ± 35	*Mt (nearshore)*	10712-10520	10627 ± 46	372.1	/	/	/
2017-PSPCA-6	SacA55426[‡]	8520 ± 35	*Mt (nearshore)*	9542-9479	9514 ± 18	348	/	/	/
Logiya_1A	Beta 446441[‡ †]	9180 ± 30	*Mt (nearshore)*	10477-10245	10330 ± 55	397.4	/	/	/
Logiya_1B	Beta 446442[‡ †]	9100 ± 30	Ch *(nearshore)*	10477-10245	10241 ± 27	397.4	/	/	/
Gasse_1*	LGD	98.8 ± 1.2	hcc	255 – 31	121 ± 78	241.7	2.5	- 0.3025	241.3975
Gasse_2*	LGD	100.6 ± 0.9	hcc	255 – 31	122 ± 78	241.7	/	/	/
Gasse_6*	LGD	110 ± 50	hcc	276 – 9	124 ± 81	266.4	/	/	/
Gasse_7*	LGD	1030 ± 100	hcc	1178 – 738	984 ± 115	266.4	/	/	/
Gasse_9*	LGD	1570 ± 60	hcc	1597 – 1337	1464 ± 63	324	/	/	/
Gasse_11*	LGD	2360 ± 80	hcc	2715 – 2160	2429 ± 140	305	/	/	/
Gasse_13*	LGD	2720 ± 120	hcc	3172 – 2490	2850 ± 55	295	/	/	/
Gasse_16*	LFR	4120 ± 110	Sh *(nearshore)*	4874 – 4297	4643 ± 144	356.8	/	/	/
Gasse_18*	LGD	4740 ± 150	*Mt (nearshore)*	5881 – 4983	5455 ± 93	364.9	/	/	/
Gasse_30*	LGD	5830 ± 140	Sh *(nearshore)*	6972 – 6316	6647 ± 167	365.6	/	/	/
Gasse_33*	LFR	5930 ± 130	Sh *(nearshore)*	7156 – 6468	6769 ± 167	365.6	/	/	/
Gasse_34*	LFR	6020 ± 160	Sh *(nearshore)*	7256 – 6501	6884 ± 196	359.6	/	/	/

Gasse_35*	LGD	6130 ± 250	*Mt (nearshore)*	7498 – 6448	7002 ± 271	337	/	/	/
Gasse_49*	LGD	6835 ± 160	*Mt (nearshore)*	7965 – 7432	7697 ± 142	381.3	/	/	/
Gasse_50*	LGD	6910 ± 180	*Mt (nearshore)*	8161 - 7429	7761 ± 161	438.2	9.1	- 70.6	367.5710
Gasse_57*	LGD	7250 ± 150	*Mt (nearshore)*	8375 – 7795	8082 ± 148	249.7	/	/	/
Gasse_62*	LFR	7450 ± 100	*Mt (nearshore)*	8416 – 8037	8263 ± 99	373.7	/	/	/
Gasse_63*	LFR	7460 ± 180	*Mt (nearshore)*	8630 – 7934	8268 ± 181	372.2	/	/	/
Gasse_64*	LFR	7610 ± 140	Sh *(nearshore)*	8770 – 8054	8420 ± 158	356.8	/	/	/
Gasse_76*	LFR	8340 ± 180	U *(nearshore)*	9704 – 8770	9302 ± 219	381.8	/	/	/
Gasse_80*	LFR	8450 ± 190	U *(nearshore)*	10129 – 8996	9434 ± 255	372.2	/	/	/
Gasse_82*	LFR	8530 ± 190	U *(nearshore)*	10154 – 9090	9545 ± 263	379.6	/	/	/
Gasse_85*	LGD	8600 ± 140	U *(nearshore)*	10151 – 9305	9633 ± 194	376.5	/	/	/
Gasse_90*	LFR	8770 ± 190	U *(nearshore)*	10273 – 9436	9848 ± 230	442.4	4.7	- 46.2	396,1144
Gasse_94*	GU	9230 ± 180	*Mt (nearshore)*	11084 – 9917	10444 ± 260	418,2	4.7	- 49	369,1132
Gasse_96*	LGD	9380 ± 130	*Mt (nearshore)*	11086 – 10253	10623 ± 216	352.1	/	/	/

Table 2

SW Footwall block				NE Axial valley				Offset	Age	Subsidence
Sample ID	Cal. Yr BP	error	Elevation (m)	Sample ID	Cal. Yr BP	error	Elevation (m)	(m)		Rate (mm/yr)
Gasse_94	10444	± 260	418,2	SacA58240	10447	± 73	369	49,2	10447	4,70948
Gasse_90	9848	± 230	442,4	SacA55608	9807	± 81	376,8	65,6	9800	6,69387
Gasse_50	7764	± 160	438,2	Poz-124783	7701	± 44	367,8	70,4	7700	9,14286